IEEE Access
Multidisciplinary | Rapid Review | Open Access Journal

Received 5 September 2022, accepted 17 October 2022, date of publication 25 October 2022, date of current version 31 October 2022.

Digital Object Identifier 10.1109/ACCESS.2022.3216876

RESEARCH ARTICLE

Fast Solution of 3-D Eddy-Current Problems in Multiply Connected Domains by a, v-φ and t-φ Formulations With Multigrid-Based Algorithm for Cohomology Generation

FEDERICO MORO[1], (Senior Member, IEEE), ARTEM NAPOV[2], MATTI PELLIKKA[3], JASMIN SMAJIC[4], (Senior Member, IEEE), AND LORENZO CODECASA[5], (Member, IEEE)

[1]Dipartimento di Ingegneria Industriale, Università degli Studi di Padova, 35131 Padua, Italy
[2]Service de Métrologie Nucléaire, Université Libre de Bruxelles, 1050 Bruxelles, Belgium
[3]Grundium Ltd., 33720 Tampere, Finland
[4]Institute of Electromagnetic Fields, Swiss Federal Institute of Technology (ETH Zürich), 8092 Zürich, Switzerland
[5]Dipartimento di Elettronica, Informazione e Bioingegneria, Politecnico di Milano, 20133 Milano, Italy

Corresponding author: Federico Moro (federico.moro@unipd.it)

Open access funding provided by the University of Padua within the CRUI-CARE Italy Read and Publish Agreement.

ABSTRACT The fast solution of three-dimensional eddy current problems is still an open problem, especially when real-size finite element models with millions of degrees of freedom are considered. In order to lower the number of degrees of freedom a magnetic scalar potential can be used in the insulating parts of the model. This may become difficult when the model geometry presents some conductive parts which are multiply connected. In this work a multigrid-based algoritm is proposed that allows for a calculation in linear-time of cohomology, which is needed to introduce the scalar potential without cuts. This algorithm relies on an algebraic multigrid solver for curl-curl field problems, which ensures optimal computational complexity. Numerical results show that the novel algorithm outperforms state-of-the-art methods for cohomology generation based on homological algebra. In addition, based on this algoritm, novel a, v-φ and t-φ formulations to analyze three-dimensional eddy current problems in multiply connected domains are proposed. Both formulations, after discretization by the cell method, lead to a complex symmetric system of linear equations amenable to fast iterative solution by Krylov-subspace solvers. These formulations are able to provide very accurate numerical results, with a minimum amount of degrees of freedoms to represent the eddy current model. In this way the computational performance is improved compared to the classical A, V-A formulation typically implemented in finite element software for electromagnetic design.

INDEX TERMS Eddy currents, AC problem, finite element method, multiply connected, electromagnetic, multigrid, cohomology.

I. INTRODUCTION

Most of commercial finite element software for electromagnetic (EM) analysis at low frequency relies on the so-called A, V-A and T-Ω formulations [1], [2]. In particular, the discretization of the A, V-A formulation by the finite element method (FEM) with edge-element vector shape functions leads to a large number of degrees of freedom (DOFs) if large-scale engineering problems are to be simulated. In addition, the final linear system resulting from edge-element discretization is poorly conditioned and can be hardly treated by state-of-the-art preconditioned Krylov (sub)space solvers. Ill-conditioning becomes even more pronounced as the number of edge DOFs increases, which is typical of FEM models of practical interest. T-Ω formulation, originally proposed in [3], makes it possible to reduce the number of edge DOFs by introducing in the whole computational domain a magnetic scalar potential Ω, approximated by nodal shape

The associate editor coordinating the review of this manuscript and approving it for publication was Guido Lombardi.

functions. This formulation poses, however, serious challenges if field problems with multiply connected domains are to be simulated because Ω is then not uniquely defined. Moreover, the electric vector potential T requires the imposition of homogeneous Dirichlet boundary conditions (BCs) on the surface of conductors to enforce the electric insulation constraint. In the case of multiply connected problems, this may lead to an incorrect enforcement of Ampère's law and thus to an erroneous eddy current reconstruction. To make the potential uniquely defined suitable cutting surfaces (known as *cuts*) can be introduced [4], [5]. The determination of cuts is however cumbersome, especially if knotted parts are present in the model geometry [6]. To the authors' knowledge, robust cut generation algorithms are presently not available; for instance, self-intersecting surfaces are typically generated by most of approaches presented in literature. An algorithm for generating cuts even with domains containing knotted parts is provided in [7]; however, it implies the preliminary knowledge of cut orientations to incorporate potential jumps.

A different strategy to make the insulating region simply-connected is to generate a *thick cut*, i.e., a layer of tetrahedrons attached to a cut and where the curl-free condition for T is strongly imposed [8]. In this case the magnetic scalar potential becomes uniquely defined and the insulation constraint can be properly imposed on conductor surfaces. Algorithms for thick cuts (see, e.g., [9], [10]) require, however, the preliminary generation of a cut, thus suffering from the lack of robustness mentioned above.

In [11] it is observed that the definition of cuts in the insulating region can be avoided if special vector fields, termed *cohomology generators* or *loop fields*, are introduced. These vector fields form a basis for the space of curl-free fields that are not gradients of a scalar potential, i.e., the *first de Rham cohomology group*, which is crucial to represent correctly the magnetic field in the insulating region. The algorithm proposed in [11] for cohomology generation relies on the concept of constrained spanning tree and requires the preliminary construction of the first homology group. Classical techniques for computing cohomology groups rely on so-called *Smith Normal Form* (SNF) integer matrix decomposition, which has the main drawback of hyper-cubical computational complexity [12]. The huge cost of cohomology computation can be alleviated, for instance, by using mesh reduction algorithms, which preserve the topological properties of the original mesh and run with super-linear computational complexity $\mathcal{O}(N \log N)$ [13]. A general homology and cohomology solver for finite element meshes, based on the rigorous mathematical framework of homological algebra, is proposed in [14]. This tool is integrated as a part of the open source mesh generation software *Gmsh* [15].

In [16] a novel approach for generating loop fields directly at the discrete level is presented. Its basic advantage is that it does not require group algebra computations for finding cohomology generators, avoiding time consuming integer matrix decomposition. By this novel algorithm a candidate curl-free field is generated by using an iterative solver for rectangular linear systems. Its complement with respect to the space of gradients is computed by an optimal algebraic multigrid solver (AGMG) and added, after orthogonalization, to the set of loop fields. These are finally used for decomposing the magnetic field at the discrete level in the insulating region. This is further used in the h-φ formulation for eddy-current problems, which makes use of edge DOFs h (i.e., magnetomotive forces along mesh edges) in the conductive parts and nodal DOFs φ (i.e., magnetic scalar potentials evaluated at mesh nodes) in the insulating region, with minimum amount of unknowns.

An alternative to the h-φ formulation is the a-φ formulation, where line integrals of the magnetic vector potential a are used as working variables, as an alternative of h variables [17]. In such a way modeling flexibility can be enhanced. For instance, edge DOFs can be used also in the insulating region to simplify its topology (e.g., by filling some holes) and in turn the number of loop fields needed to represent the magnetic field can be reduced. In addition, in [17] the computational efficiency of the algorithm for cohomology generators is improved by using an iterative multigrid solver with optimal complexity specifically designed for the solution of curl-curl field problems (AGMGcc) [18].

In this work the mutigrid algorithm for computing cohomology generators is further refined. In particular its robustness is improved by avoiding the use of Dirichlet boundary conditions. Efficiency is also improved by constructing the preconditioner of the AGMGcc solver only once, for each connected component of the interface between the interior and the exterior region. The resulting algorithm is tested against the Gmsh algorithm, which relies on state-of-the-art techniques based on homological algebra, by considering two different benchmarks with complex topology. $\mathcal{O}(N)$ time complexity is also illustrated by considering different mesh refinements of the same discretized benchmark models.

Moreover, by exploiting the new multigrid-based algorithm, two novel formulations are proposed, allowing to significantly improve the efficiency of previous formulations based on the use of magnetic scalar potential. These novel formulations are inspired by the so-called *hybrid formulations*, which combine differential and integral discretization approaches such as the cell method (CM) and the boundary element method (BEM) [19]. The first approach is the electric a, v-φ formulation, which makes use of additional nodal DOFs (i.e., electric potentials evaluated at mesh nodes v) in the interior domain. Numerical experiments show that, although the number of DOFs is increased, the computational performance is improved with respect to a-φ method already presented. Moreover, unlike the classical A, V-A method, the electric scalar potential can be used also (if needed) in the insulating region. In a similar fashion, a magnetic t-φ formulation is presented as an alternative of the h-φ method, with excellent computational performance. In this case the use of magnetic scalar potential is extended to the whole computational domain to allow for the decomposition of h variables in the conductive region. It has to be noted that the

main difference with the classical T-Ω formulation is that insulating condition is not explicitly imposed on conductors, while retaining modeling accuracy.

The paper is organized as follows. Electric and magnetic formulations for 3-D eddy-current problems are first presented in the continuous setting in Section II. The novel algorithm for generating loop fields, based on the AGMGcc multigrid iterative solver with optimal complexity, is presented in Section III. The discretization of electric and magnetic formulations by the CM is presented in Section IV. Finally, these formulations are tested against benchmarks with complex topology in Section V, aiming at showing computational performance and accuracy level in comparison with numerical results from a second-order FEM software.

II. EDDY-CURRENT PROBLEM

EM field problems at low frequency can be described by neglecting wave propagation and taking into account only diffusion inside electric and magnetic media. Maxwell's equations obtained by disregarding the displacement current are expressed in the frequency domain as:

$$\nabla\times\mathbf{E}+\imath\,\omega\mathbf{B}=\mathbf{0}, \tag{1}$$
$$\nabla\times\mathbf{H}=\mathbf{J}, \tag{2}$$
$$\mathbf{J}=\sigma\mathbf{E}+\mathbf{J}_0, \tag{3}$$
$$\mathbf{H}=\nu\mathbf{B}, \tag{4}$$

where $\imath$ is the imaginary unit, ω is the angular frequency. Material parameters are the electric conductivity σ and the magnetic reluctivity ν. The part of Ω in which $\sigma>0$ is the conductive region, denoted as Ω_C. ν is defined throughout Ω (in particular, ν_0 indicates the air reluctivity). Both material parameters are assumed to be piecewise constants and may be subject to local spatial variations (e.g., presence of inhomogeneous magnetic and/or conductive materials). The electric field $\mathbf{E}$, the magnetic flux density $\mathbf{B}$, and the magnetic field $\mathbf{H}$ are defined in the computational domain Ω. The current density $\mathbf{J}$ is split as a sum of the eddy current density $\sigma\mathbf{E}$ and the source current density $\mathbf{J}_0$. The latter represents current-driven coils in the source region Ω_0, where $\sigma=0$ is assumed as the skin effect is generally neglected there.

By taking the divergence of (1) and (2), the magnetic and the electric conservation equations are obtained:

$$\nabla\cdot\mathbf{B}=0, \tag{5}$$
$$\nabla\cdot\mathbf{J}=0. \tag{6}$$

Scalar potential formulations here proposed are derived in the same spirit of hybrid formulations [19], [20], [21] combining different discretization approaches such as CM and BEM or FEM and BEM, with the following main features: i) Ω is partitioned into interior and exterior field problems, ii) a vector potential is used as a main unknown in the interior region, and iii) a scalar potential is used in the exterior region.

In the following electric and magnetic formulations, based on the magnetic scalar potential, are obtained by coupling EM formulations of both exterior and interior field problems.

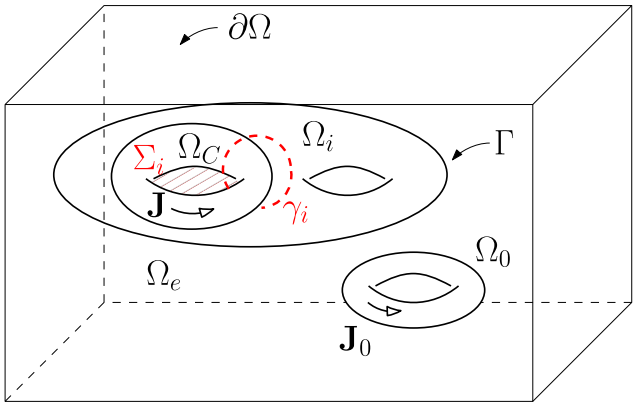

FIGURE 1. Computational domain for defining the electric formulation based on the magnetic vector potential.

Fig. 1 shows the computational domain Ω used for defining the electric formulation: the interior region Ω_i (an open and bounded subset of Ω) is modeled by using the magnetic vector potential, whereas Ω_e is modeled by using the scalar potential; the source region Ω_0 with current-driven coils is contained outside Ω_i; the insulating region is bounded by $\partial\Omega$, i.e., the computational domain boundary.

A. EXTERIOR PROBLEM

The exterior region is the complement of the interior region in the computational domain, i.e. $\Omega_e=\Omega\setminus\overline{\Omega}_i$, where $\overline{\Omega}_i$ indicates the set closure of Ω_i. In the most general case, with an arbitrary topological setting, the exterior region may be multiply connected. It means that there exists a loop in Ω_e which cannot be shrink to a point while remaining in Ω_e [5].

The most simple way to model the magnetostatic problem in Ω_e is to consider the electric field diffusion equation (16) for $\sigma=0$, leading to the so-called A-A formulation [2]. In the similar fashion, starting from diffusion equation (17), the A, V-A formulation is obtained. Also in this case A is used in the insulating region. Both these electric formulations are typically discretized by using edge-element shape functions, with the main drawback of a huge number of DOFs in engineering problems of practical interest.

The best solution in order to minimize the number of DOFs in Ω_e is to use a magnetic scalar potential, since by using nodal shape functions DOFs are related to the mesh nodes instead of mesh edges unlike previous formulations. If Ω_e is multiply connected the magnetic scalar potential φ is not uniquely defined in Ω_e due to eddy current flowing in Ω_i. This is illustrated in Fig. 1 by a simple example: a loop γ_i, embracing the torus Ω_C, is intersecting a cut Σ_i (depicted in shaded line in Fig. 1). Since Σ_i makes the insulating region simply connected, the potential is uniquely defined in $\Omega_e\setminus\Sigma_i$, together with its gradient $\nabla\varphi$, and Ampère's law on γ_i reads:

$$I_i=\int_{\gamma_i}\mathbf{H}\cdot\,d\mathbf{l}=\int_{\gamma_i}\nabla\varphi\cdot\,d\mathbf{l}=[\varphi]_{\Sigma_i}, \tag{7}$$

where I_i is the eddy current flowing in Ω_C and square brackets indicate the potential jump across Σ_i. Cuts and loops are dual to each other thanks to Poincaré duality [22]. The construction of cuts (dubbed as *Seifert surfaces* in topology) is however complex and computationally intensive [5]. An alternative approach, discussed below, avoiding the use of cuts and potential jumps as (7), will be adopted here.

In order to avoid cuts the use of cohomology generators, filling the space of curl-free fields that are not gradients, was first proposed by Henrotte in [11]. By this approach the magnetic field in Ω_e is split as follows:

$$\mathbf{H} = \nabla\varphi + \sum_{k=1}^{\beta_1} I_k \, \mathbf{H}_k, \tag{8}$$

where I_k are currents in independent circuits to be identified in Ω_i, and $\mathbf{H}_k$, $k = 1, \ldots, \beta_1$, with β_1 first-order Betti number of Ω_i, is the cohomology basis. I_k can be either induced currents (e.g., as the current flowing in Ω_C, in Fig. 1) or impressed currents in coils. The main limitation of this approach is that both independent cuts and a constrained spanning-tree need to be constructed in Ω_i. In [14] this is avoided by using tools from homological algebra to compute cohomology; however, unlike (8), DOFs related to loop fields are linear combinations with integers coefficients of I_k.

In this work a magnetic field decomposition, which does not rely on cuts in Ω_i such as (8), is adopted (see, e.g., [5]):

$$\mathbf{H} = \mathbf{H}_0 + \nabla\varphi + \sum_{k=1}^{\beta_1} \xi_k \, \mathbf{T}_k, \tag{9}$$

where ξ_k are DOFs without physical significance that are determined when solving the final linear system, after numerical discretization. Vector fields $\mathbf{T}_k$, $k = 1, \ldots, \beta_1$ form the cohomology basis in Ω_i (which is indicated differently from (8) since generators are unconstrained). $\mathbf{H}_0$ is the so-called *source field*, i.e., any field which fulfills Ampère's law:

$$\nabla\times \mathbf{H} = \mathbf{J}_0. \tag{10}$$

The source field is typically constructed at the pre-processing stage; then magnetic field sources such as current-driven coils are eliminated from the computational domain.

The algorithms presented, e.g., in [5] or [14] are based, however, on the SNF decomposition, which involves high computational complexity [23]. An algorithm computing directly cohomology, which avoids integer computations and does not take any mesh manipulation, is presented in [16]. An improved version of this algorithm, relying on an algebraic multigrid iterative solver with preconditioner setup, is discussed in Section III. The key idea of the multigrid-based approach, introduced in [17], is to construct in linear-time the cohomology group directly at the algebraic level by solving an equivalent magnetostatic linear systems with multigrid.

Topological constraints for enforcing ξ_k, $k = 1, \ldots, \beta_1$, are derived by applying the *virtual work principle* in Ω_e as shown in [19]. By assuming $\mathbf{A}\times\mathbf{n} = \mathbf{0}$ on the domain boundary $\partial\Omega$ (see Fig. 1), i.e., magnetic wall BCs, the following condition is obtained:

$$\int_{\Omega_e} \mathbf{T}_k \cdot \mathbf{B} \, d\Omega + \int_{\Gamma} \mathbf{A} \cdot \mathbf{T}_k \times \mathbf{n} \, d\Gamma = 0, \tag{11}$$

with $k = 1, \ldots, \beta_1$ and $\mathbf{n}$ is the outward unit normal on the interface Γ pointing out from Ω_i.

By inserting the magnetic field decomposition (9) in the magnetic constitutive relationship:

$$\mathbf{B} = \mu \, \mathbf{H}, \tag{12}$$

where $\mu = \nu^{-1}$ is the magnetic permeability, and by using (5), one obtains Poisson's equation which governs the magnetostatic problem in the exterior domain:

$$-\nabla\cdot \mu \, \nabla\varphi = \nabla\cdot \mu\mathbf{H}_0 + \sum_{k=1}^{\beta_1} \xi_k \nabla\cdot \mu\mathbf{T}_k. \tag{13}$$

The exterior problem is eventually solved by assuming homogeneous Neumann BCs on the computational domain boundary $\partial\Omega$ and suitable interface conditions on Γ.

B. INTERIOR PROBLEM

Two different modeling approaches for modeling the field problem in the interior region are presented in this section.

In the so-called *electric formulation* the electric field diffusion in Ω_i is described in terms of a magnetic vector potential $\mathbf{A}$ such that:

$$\mathbf{E} = -\imath \, \omega\mathbf{A}. \tag{14}$$

The interior region, in which $\mathbf{A}$ is defined, may include also non-conductive materials, i.e., $\Omega_C \subseteq \Omega_i$ (see, e.g., Fig. 1).

Since it is assumed also that the source domain is contained outside Ω_i, it results $\mathbf{J}_0 = \mathbf{0}$ in (3). The conservation equation (5) can be expressed in terms of potential as:

$$\mathbf{B} = \nabla\times \mathbf{A}, \tag{15}$$

where $\mathbf{A}$ is defined up to a gradient of a scalar function. By letting (14) in (3), with $\mathbf{J}_0 = \mathbf{0}$, and (15) in (4), the magnetic diffusion equation in Ω can be derived from (2) as:

$$\nabla\times \nu\nabla\times \mathbf{A} + \imath \, \omega\sigma \, \mathbf{A} = \mathbf{0}. \tag{16}$$

By using the gauge transformation $\mathbf{A} \mapsto \mathbf{A} + \nabla v$, where v is the primitive (i.e., time integral) of the electric scalar potential, (16) can be expressed in this equivalent form:

$$\nabla\times \nu\nabla\times \mathbf{A} + \imath \, \omega\sigma \, (\mathbf{A} + \nabla v) = \mathbf{0}. \tag{17}$$

The potential v is constrained in Ω_C by imposing the electric conservation equation (6), together with (3), as:

$$-\imath \, \omega\nabla\cdot \sigma \, (\mathbf{A} + \nabla v) = 0. \tag{18}$$

The other possibility is to describe magnetic diffusion in Ω_C by using the magnetic field as working variable, thus obtaining the so-called *magnetic formulation*. In this case the interior domain is restricted to the conductive region, i.e.,

$\Omega_i = \Omega_C$, and cannot include magnetic materials, unlike the electric formulation. The computational domain of the magnetic formulation can be depicted similar to Fig. 1.

By taking $\mathbf{J}_0 = \mathbf{0}$ following the same argument as above, the electric constitutive equation (3) becomes:

$$\mathbf{E} = \rho\,\mathbf{J}, \tag{19}$$

where $\rho = \sigma^{-1}$ is the electrical resistivity. By letting (19) and (12) in (1), and by using (2), one obtains the magnetic diffusion equation in terms of the magnetic field variable:

$$\nabla\times\,\rho\nabla\times\,\mathbf{H} + \imath\,\omega\,\mu\,\mathbf{H} = \mathbf{0}, \tag{20}$$

which, unlike (16), holds only if $\sigma > 0$, i.e., inside Ω_C. By using the gauge transformation $\mathbf{H} \mapsto \mathbf{T} + \nabla\varphi$, with $\mathbf{T}$ electric vector potential, the equivalent form of (20) reads:

$$\nabla\times\,\rho\nabla\times\,\mathbf{T} + \imath\,\omega\,\mu\,\,(\mathbf{T} + \nabla\varphi) = \mathbf{0}. \tag{21}$$

Potential φ is constrained in the whole domain Ω by imposing the conservation equation (5), together with (12), as:

$$\nabla\cdot\,\mu\,(\mathbf{T} + \nabla\varphi) = 0. \tag{22}$$

III. COHOMOLOGY BY MULTIGRID-BASED ALGORITHM

Interior and exterior field problems in the continuous setting are discretized by using the CM. Details of this discretization method, alternative to FEM, are given in [17] or [19] and are here briefly summarized. The computation domain is meshed into tetrahedral cells and any subdomain Ω_d, $d \in \{C, i, e, 0\}$, is discretized by its mesh partition $\mathcal{G}_{\Omega_d}$, i.e., the *primal grid*, and the corresponding *dual grid* $\widetilde{\mathcal{G}}_{\Omega_d}$ obtained by joining tetrahedrons of the barycentric dual complex related to $\mathcal{G}_{\Omega_d}$. Any physical field can be approximated by using an array of DOFs, termed *discrete field*, whose coefficients are related to geometric entities of either primal or dual grids (i.e., potential on nodes, line integrals, and fluxes through faces). Differential operators are approximated as incidence matrices. Constitutive relationships are approximated (after a suitable choice of shape functions) as positive-definite matrices. A linear system is finally assembled and solved.

By integrating (9) along each primal edge of $\mathcal{G}_{\Omega_e}$ and by using Stokes' theorem, the corresponding magnetic discrete field decomposition is obtained:

$$\mathbf{h}_{\Omega_e} = \mathbf{h}_{0,\Omega_e} + \mathbf{G}_{\Omega_e}\,\boldsymbol{\varphi}_{\Omega_e} + \sum_{k=1}^{\beta_1}\xi_k\,\mathbf{t}_{k,\Omega_e}, \tag{23}$$

where $\mathbf{h}_{\Omega_e} = (h_e)_{e\in\mathcal{G}_{\Omega_e}}$ is the array of magnetomotive forces (mmfs) $h_e = \int_e \mathbf{H}\cdot d\mathbf{l}$, i.e. line integrals of $\mathbf{H}$ along any edge e of $\mathcal{G}_{\Omega_e}$, and the other arrays of edge DOFs $\mathbf{h}_{\Omega_e}$, $\mathbf{h}_{0,\Omega_e}$, and $\mathbf{t}_{k,\Omega_e}$ are defined in a similar fashion. The edge-to-node incidence matrix of $\mathcal{G}_{\Omega_e}$, or discrete gradient, $\mathbf{G}_{\Omega_e}$, is made up by $0, \pm 1$ coefficients and it is obtained by applying Stokes' theorem to the gradient in (9). Finally, $\boldsymbol{\varphi}_{\Omega_e}$ is the array of magnetic scalar potential evaluations on the primal nodes of $\mathcal{G}_{\Omega_e}$, i.e. $\boldsymbol{\varphi}_{\Omega_e} = (\varphi(n))_{n\in\mathcal{G}_{\Omega_e}}$. It has to be noted that the number of generators in (23) equals that in (9), due to de Rham theorem which establishes an isomorphism between de Rham cohomology (related to physical fields, in the continuous setting) and singular cohomology (related to discrete fields, obtained after CM discretization) [24].

In this work an improved version of the algorithm proposed in [16] is proposed. The original algebraic procedure was able to avoid the generation of the homology basis (requiring time-consuming mesh data manipulations) and to compute the discrete cohomology basis $\mathbf{t}_{k,\Omega_e}$ by solving rectangular linear systems with iterative solvers such as LSMR or LSQR. The main advantage of the new algorithm is to rely on an algebraic multigrid iterative solver in order to guarantee (optimal) linear-time complexity in the generation of cohomology, which had not been obtained before.

The starting point of this algorithm is to observe from (23) that discrete cohomology generators $\mathbf{t}_{k,\Omega_e}$ are curl-free, in the sense that they lie in the kernel of face-to-edge incidence matrix of $\mathcal{G}_{\Omega_e}$, or discrete curl, $\mathbf{C}_{\Omega_e}$. In fact, by applying the curl operator to (23), the discrete source field $\mathbf{h}_{0,\Omega_e}$ fulfills:

$$\mathbf{C}_{\Omega_e}\mathbf{h}_{\Omega_e} = \mathbf{j}_{0,\Omega_e}, \tag{24}$$

and the matrix identity $\mathbf{C}_{\Omega_e}\mathbf{G}_{\Omega_e} = \mathbf{0}$ holds, i.e., the discrete counterpart of vector identity $\nabla\times\nabla(\cdot) = \mathbf{0}$. (24) is obtained by integrating (10) on the faces of $\mathcal{G}_{\Omega_e}$ and by using Stokes' theorem. $\mathbf{j}_{0,\Omega_e} = (j_{0,f})_{f\in\mathcal{G}_e}$ is the array of source currents $j_{0,f} = \int_f \mathbf{J}_0\cdot d\mathbf{s}$, i.e. fluxes of $\mathbf{J}_0$ thorough any face f of $\mathcal{G}_{\Omega_e}$. Therefore, any candidate generator is a vector $\mathbf{u}_{\Omega_e}$ such that $\mathbf{C}_{\Omega_e}\mathbf{u}_{\Omega_e} = \mathbf{0}$. As proven in [17], this corresponds to solve the following (square) equivalent magnetostatic system:

$$\mathbf{C}_{\Omega_e}^{\mathrm{T}}\mathbf{C}_{\Omega_e}\mathbf{u}_{\Omega_e} = \mathbf{0}, \tag{25}$$

where $(\cdot)^{\mathrm{T}}$ indicates the matrix transpose. It is shown in Section V that (25), which is built at negligible computing cost, can be solved with optimal computational complexity by using the AGMGcc iterative solver.

AGMGcc solver [18] is intended for the solution of curl-curl linear systems like (25). The solver is based on the flexible variant of the conjugate gradient method [25] used with an auxiliary space preconditioner inspired by [26] and [27]. The preconditioner combines the successive application of the symmetrized Gauss-Seidel iterative scheme with an approximate solution of some auxiliary linear systems. The auxiliary systems are obtained by projecting the original curl-curl linear system into discrete H^1 auxiliary spaces, and are solved using the block variant of AGMG solver [28]. Note that with AGMGcc solver the setup of the preconditioner and the linear system solution based on the preconditioner can be performed separately.

The second step is to observe that $\mathbf{t}_{k,\Omega_e}$ are curl-free fields that are not in the range of $\mathbf{G}_{\Omega_e}$; therefore, generators can be obtained by considering any $\mathbf{v}_{\Omega_e} = \mathbf{u}_{\Omega_e} - \mathbf{G}_{\Omega_e}\boldsymbol{\varphi}_{\Omega_e}$ which is orthogonal to the columns of $\mathbf{G}_{\Omega_e}$. It is shown in [16] that this amounts to solve the square Poisson-like linear system:

$$\mathbf{G}_{\Omega_e}^{\mathrm{T}}\mathbf{M}_{\mu,\Omega_e}\mathbf{G}_{\Omega_e}\,\boldsymbol{\varphi}_{\Omega_e} = \mathbf{G}_{\Omega_e}^{\mathrm{T}}\mathbf{M}_{\mu,\Omega_e}\mathbf{u}_{\Omega_e}, \tag{26}$$

where $\mathbf{M}_{\mu,\Omega_e}$ is the (positive definite) magnetic constitutive matrix of $\mathcal{G}_{\Omega_e}$, built by using piecewise uniform edge basis functions [29]. Linear system (26) can be solved again very efficiently in linear-time by an algebraic multigrid iterative solver (AGMG) for grad-grad discrete problems [28].

Last step of the multigrid-based algorithm is to extract an orthogonal basis by using a QR decomposition algorithm with column update. This ensures that cohomology generators are linearly independent from each other and thus form a basis. These are stored column-wise in the so-called *cohomology matrix*:

$$\mathbf{T}_{\Omega_e} = \left[\mathbf{t}_{1,\Omega_e}, \ldots, \mathbf{t}_{\beta_1,\Omega_e}\right]. \tag{27}$$

Basic steps of the multigrid-based algorithm are summarized by Algorithm 1 and discussed point by point in the following.

Algorithm 1 (Cohomology in Linear Time)

1: Init cohomology matrix $\mathbf{T}_{\Omega_e} = [\,]$
2: Init stiffness matrix $\mathbf{K} = \mathbf{C}_{\Omega_e}^{\mathrm{T}}\mathbf{C}_{\Omega_e}$
3: Find connected components $\mathcal{G}_\Gamma^{(m)}$ of $\mathcal{G}_\Gamma$, $m = 1, \ldots, M$
4: Init number of generators $k = 0$
5: Init interface genus $g = 0$
6: **for** $m = 1, \ldots, M$ **do**
7: $\quad\chi_m = N_\Gamma^{(m)} - E_\Gamma^{(m)} + T_\Gamma^{(m)}$
8: $\quad$Init component genus $g_m = 1 - \chi_m/2$
9: $\quad g = g + g_m$
10: $\quad$Preconditioner setup for (25)
11: $\quad$**if** $g_m > 0$ **then**
12: $\quad\quad$Init set $\mathcal{E}_\Gamma^{(m)}$ of g_m edges pick randomly on $\mathcal{G}_\Gamma^{(m)}$
13: $\quad\quad$**while** $k < g$ **do**
14: $\quad\quad\quad$Init perturbation vector $\delta\mathbf{u}_{\Omega_e} = \mathbf{0}$
15: $\quad\quad\quad$Set $\delta\mathbf{u}_{\Omega_e,j}$ to random value for any $j \in \mathcal{E}_\Gamma^{(m)}$
16: $\quad\quad\quad$Init $\mathbf{f} = -\mathbf{K}\,\delta\mathbf{u}_{\Omega_e}$
17: $\quad\quad\quad$Solve $\mathbf{K}\,\widehat{\mathbf{u}}_{\Omega_e} = \mathbf{f}$
18: $\quad\quad\quad\mathbf{u}_{\Omega_e} = \widehat{\mathbf{u}}_{\Omega_e} + \delta\mathbf{u}_{\Omega_e}$
19: $\quad\quad\quad$Compute the orthogonal complement $\mathbf{v}_{\Omega_I}$ of $\mathbf{u}_{\Omega_e}$ with respect to the range of $\mathbf{G}_{\Omega_e}$
20: $\quad\quad\quad$Compute the orthogonal complement $\mathbf{w}_{\Omega_e}$ of $\mathbf{v}_{\Omega_e}$ with respect to the range of $\mathbf{T}_{\Omega_e}$
21: $\quad\quad\quad$**if** $\|\mathbf{w}_{\Omega_e}\|_\mu > 0$ **then**
22: $\quad\quad\quad\quad k = k + 1$
23: $\quad\quad\quad\quad\mathbf{t}_{k,\Omega_e} = \mathbf{w}_{\Omega_e}/\|\mathbf{w}_{\Omega_e}\|_\mu$
24: $\quad\quad\quad\quad\mathbf{T}_{\Omega_e} = \left[\mathbf{T}_{\Omega_e}, \mathbf{t}_{k,\Omega_e}\right]$
25: $\quad\quad\quad$**end if**
26: $\quad\quad$**end while**
27: $\quad$**end if**
28: **end for**

It has to be noted first that the number of cohomology generators β_1 equals the interface genus g. In fact, the number of homology generators of Ω_e (which is β_1, as cohomology) is equal to that of Ω_i, for the Alexander duality, and the union of generators forms the homology group of Γ, whose dimension is $2g$ (see, e.g, [23]). From this observation, cohomology is here extracted by considering edges lying on the connected components $\mathcal{G}_\Gamma^{(m)}$ of $\mathcal{G}_\Gamma$, i.e., the interface primal grid.

At line 1, $\mathbf{T}_{\Omega_e}$ is initialized to the empty matrix.

At line 2, the stiffness matrix of the linear system (25) is built.

At line 3 $\mathcal{G}_\Gamma^{(m)}$, $m = 1, \ldots, M$, are identified on $\mathcal{G}_\Gamma$.

At line 8, for any mth component, the genus g_m of $\mathcal{G}_\Gamma^{(m)}$ is computed from its Euler's characteristic χ_m. Cohomology generators for that component are extracted only if $g_m > 0$, i.e., in the case of non-trivial surface topology.

At line 10, the AGMGcc preconditioner for the linear system (25) is built and stored once for each connected component of Γ. This allows to speed up computations since (25) has to be solved g_m times at least.

At line 12, g_m edges are randomly picked from $\mathcal{G}_\Gamma^{(m)}$. For any edge a random value is assigned at line 15. These values are the non-zero coefficients of the perturbation vector $\delta\mathbf{u}_{\Omega_e}$.

At line 18, an admissible curl-free field $\mathbf{u}_{\Omega_e}$ is found by solving (25) with AGMGcc solver (line 17). In order to obtain a non-trivial solution the non-trivial RHS is formed from perturbation vector (line 16). The key idea of the algorithm is that random DOFs, set on interface edges, force the solver to search for a non-trivial $\mathbf{u}_{\Omega_e}$. It has to be noted that this solution strategy is different from that used in the former version of the algorithm [16], which often led to failures of AGMGcc because of the use of Dirichlet BCs, and it has been specifically designed to ensure robustness and fast convergence behavior to AGMGcc solver.

At line 19, the orthogonal complement $\mathbf{v}_{\Omega_e}$ of $\mathbf{u}_{\Omega_e}$ with respect to the range of $\mathbf{G}_{\Omega_e}$ is found by solving (26) with AGMG iterative solver.

At line 20, the orthogonal complement $\mathbf{w}_{\Omega_e}$ of $\mathbf{v}_{\Omega_e}$ with respect to the range of $\mathbf{T}_{\Omega_e}$ is found by using a QR decomposition algorithm with column update.

At line 21, a linear dependency check on orthogonal complement is realized: If its energy norm

$$\|\mathbf{w}_{\Omega_I}\|_\mu = \sqrt{\mathbf{w}_{\Omega_e}^{\mathrm{T}}\mathbf{M}_{\mu,\Omega_e}\mathbf{w}_{\Omega_e}}, \tag{28}$$

is non-zero, then $\mathbf{w}_{\Omega_e}$ is linearly independent with respect to previous generators and can be added to the cohomology matrix after normalization (lines 23-24). By noting that any $\mathbf{v}_{\Omega_e}$ is orthogonal to the range of $\mathbf{G}_{\Omega_e}$ and any $\mathbf{t}_{k,\Omega_e}$ is a linear combination of these vectors, it readily follows that:

$$\mathbf{G}_{\Omega_e}^{\mathrm{T}}\mathbf{M}_{\mu,\Omega_e}\mathbf{T}_{\Omega_e} = \mathbf{0}, \tag{29}$$

that is orthogonality holds also for cohomology generators.

Iterations stops at line 26 when $k = g$, i.e., a number of g_m cohomology generators has been extracted for $\mathcal{G}_\Gamma^{(m)}$.

IV. HYBRID FORMULATIONS

Maxwell's equations in the frequency domain, described in Section II, are discretized by using the CM. Because interior and exterior problems are discretized separately and then interfaced by continuity constraints, similarly to hybrid methods combining different numerical techniques, electric

(a-φ and a, v-φ) and magnetic formulations (h-φ and t-φ), presented in the following, are termed *hybrid formulations*. a-φ and h-φ formulations have already been derived in [17] and [16], respectively, and are here briefly recalled for the sake of clarity and completeness. Starting from these bases, novel a, v-φ and t-φ formulations, with improved numerical performances, are obtained in Section IV-C and IV-D.

A. DISCRETE SOURCE FIELD

The discrete source field $\mathbf{h}_{0,\Omega_e}$, which represents the field sources in $\mathcal{G}_{\Omega_e}$, can be found by solving the linear system:

$$\mathbf{C}_{\Omega_e}^{\mathrm{T}}\mathbf{C}_{\Omega_e}\mathbf{h}_{0,\Omega_e} = \mathbf{C}_{\Omega_e}^{\mathrm{T}}\mathbf{j}_{0,\Omega_e} \tag{30}$$

which is equivalent to (24), as proven in [17]. This linear system can be solved efficiently by using AGMGcc solver. From numerical experiments it can be however observed that multigrid convergence can be accelerated by considering (30) on the whole domain, instead of exterior region only. In this case $\mathbf{h}_{0,\Omega_e}$ is simply the solution restriction to $\mathcal{G}_{\Omega_e}$. It has to be pointed out that this new approach for finding the source field can be applied to meshes with millions of elements, with a limited computational effort (see results in Section V).

B. CM FORMULATION IN EXTERIOR REGION

The magnetostatic problem in the exterior region is discretized in the same way for both electric and magnetic hybrid formulations. By integrating the magnetic conservation equation (5) on each cell of $\widetilde{\mathcal{G}}_{\Omega_e}$ and by applying the divergence theorem, one obtains:

$$\widetilde{\mathbf{D}}_{\Omega_e}\widetilde{\mathbf{b}}_{\Omega_e} - \widetilde{\mathbf{D}}_{\Omega_e\Gamma}\widetilde{\mathbf{b}}_{\Gamma} = \mathbf{0}, \tag{31}$$

where $\widetilde{\mathbf{b}}_{\Omega_e} = (b_{\widetilde{f}})_{\widetilde{f}\in\widetilde{\mathcal{G}}_{\Omega_i}}$ is the array of magnetic fluxes $b_{\widetilde{f}} = \int_{\widetilde{f}} \mathbf{B}\cdot d\mathbf{s}$ through any face $\widetilde{f}$ of $\widetilde{\mathcal{G}}_{\Omega_e}$ and $\widetilde{\mathbf{b}}_{\Gamma}$ is the array of magnetic fluxes through the faces of $\widetilde{\mathcal{G}}_{\Gamma}$, computed with Γ oriented by a unit normal $\mathbf{n}$, pointing out from Ω_i. The minus sign in (31) accounts for the opposite orientation of Γ and $\partial\Omega_e$, on which the divergence theorem is applied. $\widetilde{\mathbf{D}}_{\Omega_e}$ is the volume-to-face incidence matrix of $\widetilde{\mathcal{G}}_{\Omega_e}$, or dual discrete divergence, and $\widetilde{\mathbf{D}}_{\Omega_e\Gamma}$ is the surface divergence matrix, i.e., the transpose of the selection matrix (made up of 0, 1 coefficients) which extracts primal nodes of $\mathcal{G}_{\Gamma}$ from those of $\mathcal{G}_{\Omega_e}$. Bulk fluxes in (31) can be expressed as a function of mmfs by means of the magnetic constitutive relationship:

$$\widetilde{\mathbf{b}}_{\Omega_e} = \mathbf{M}_{\mu,\Omega_e}\mathbf{h}_{\Omega_e}. \tag{32}$$

By letting (23) in (32) and by using the topological identity $\widetilde{\mathbf{D}}_{\Omega_e} = -\mathbf{G}_{\Omega_e}^{\mathrm{T}}$, together with orthogonality condition (29), the discrete magnetic flux conservation (31) becomes:

$$\mathbf{G}_{\Omega_e}^{\mathrm{T}}\mathbf{M}_{\mu,\Omega_e}\mathbf{G}_{\Omega_e}\boldsymbol{\varphi}_{\Omega_e} + \widetilde{\mathbf{D}}_{\Omega_e\Gamma}\widetilde{\mathbf{b}}_{\Gamma} = -\mathbf{G}_{\Omega_e}^{\mathrm{T}}\mathbf{M}_{\mu,\Omega_e}\mathbf{h}_{0,\Omega_e}. \tag{33}$$

Topological constraints (11) can be discretized by expanding fields $\mathbf{B}$ and $\mathbf{A}$ with face and edge piecewise uniform basis functions [29]. The following relationship is obtained in [17]:

$$\mathbf{T}_{\Omega_e}^{\mathrm{T}}\left(\widetilde{\mathbf{b}}_{\Omega_e} - \widetilde{\mathbf{C}}_{\Omega_e\Gamma}\,\widetilde{\mathbf{a}}_{\Gamma}\right) = \mathbf{0}, \tag{34}$$

where $\widetilde{\mathbf{a}}_{\Gamma} = (a_{\widetilde{e}})_{\widetilde{e}\in\widetilde{\mathcal{G}}_{\Gamma}}$ is the array of magnetic vector potential line integrals $a_{\widetilde{e}} = \int_{\widetilde{e}} \mathbf{A}\times\mathbf{n}\cdot d\mathbf{l}$ along the edges of $\widetilde{\mathcal{G}}_{\Gamma}$. By letting (23) in (32), (34) can be rewritten as:

$$\mathbf{T}_{\Omega_e}^{\mathrm{T}}\left(\mathbf{M}_{\mu,\Omega_e}\mathbf{T}_{\Omega_e}\boldsymbol{\xi}_{\Omega_e} - \widetilde{\mathbf{C}}_{\Omega_e\Gamma}\,\widetilde{\mathbf{a}}_{\Gamma}\right) = -\mathbf{T}_{\Omega_e}^{\mathrm{T}}\mathbf{M}_{\mu,\Omega_e}\mathbf{h}_{0,\Omega_e}. \tag{35}$$

C. ELECTRIC HYBRID FORMULATIONS

By integrating (14) along the edges of $\mathcal{G}_{\Omega_i}$, one obtains:

$$\mathbf{e}_{\Omega_i} = -\imath\,\omega\,\mathbf{a}_{\Omega_i} \tag{36}$$

where $\mathbf{e}_{\Omega_i}$ is the array of electromotive forces (emfs) and $\mathbf{a}_{\Omega_i}$ is the array of line integrals of magnetic vector potential, both along the edges of $\mathcal{G}_{\Omega_i}$. The magnetic conservation equation in discrete form is obtained by integrating (15) on the faces of $\mathcal{G}_{\Omega_i}$ and by applying Stokes' theorem:

$$\mathbf{b}_{\Omega_i} = \mathbf{C}_{\Omega_i}\mathbf{a}_{\Omega_i}, \tag{37}$$

where $\mathbf{b}_{\Omega_i}$ is the array of magnetic fluxes through faces of $\mathcal{G}_{\Omega_i}$ and $\mathbf{C}_{\Omega_i}$ is the curl-matrix of the interior domain.

Electric and magnetic constitutive equations are obtained, as detailed in [19], by approximating local relationships (3) and (4) with piecewise uniform shape functions. Constitutive relationships at the discrete level become:

$$\widetilde{\mathbf{j}}_{\Omega_i} = \mathbf{M}_{\sigma,\Omega_i}\mathbf{e}_{\Omega_i}, \tag{38}$$

$$\widetilde{\mathbf{h}}_{\Omega_i} = \mathbf{M}_{\nu,\Omega_i}\mathbf{b}_{\Omega_i}, \tag{39}$$

where $\widetilde{\mathbf{j}}_{\Omega_i} = (j_{\widetilde{f}})_{\widetilde{f}\in\widetilde{\mathcal{G}}_{\Omega_i}}$ is the array of currents $j_{\widetilde{f}} = \int_{\widetilde{f}}\mathbf{J}\cdot d\mathbf{s}$ through faces $\widetilde{f}$ of $\widetilde{\mathcal{G}}_{\Omega_i}$ and $\widetilde{\mathbf{h}}_{\Omega_i} = (h_{\widetilde{e}})_{\widetilde{e}\in\widetilde{\mathcal{G}}_{\Omega_i}}$ is the arrays of mmfs $h_{\widetilde{e}} = \int_{\widetilde{e}}\mathbf{H}\cdot d\mathbf{l}$ along any edge $\widetilde{e}$ of $\widetilde{\mathcal{G}}_{\Omega_i}$. The conductance $\mathbf{M}_{\sigma,\Omega_i}$ and the reluctance $\mathbf{M}_{\nu,\Omega_i}$ positive-definite matrices are obtained, respectively, by using edge and face piecewise uniform bases, as discussed in [19]. Coefficients of $\mathbf{M}_{\sigma,\Omega_i}$ are non-zero only in correspondence of the edges of $\mathcal{G}_{\Omega_C}$. By integrating (2) along faces of $\widetilde{\mathcal{G}}_{\Omega_i}$ and by using again Stokes' theorem, one obtains the discrete Ampère's law:

$$\widetilde{\mathbf{C}}_{\Omega_i}\widetilde{\mathbf{h}}_{\Omega_i} + \widetilde{\mathbf{C}}_{\Omega_i\Gamma}\widetilde{\mathbf{h}}_{\Gamma} = \widetilde{\mathbf{j}}_{\Omega_i}, \tag{40}$$

where $\widetilde{\mathbf{C}}_{\Omega_i} = \mathbf{C}_{\Omega_i}^{\mathrm{T}}$ is the face-to-edge incidence matrix of $\widetilde{\mathcal{G}}_{\Omega_i}$, or dual discrete curl, and $\widetilde{\mathbf{C}}_{\Omega_i\Gamma}$ is the surface curl matrix, i.e., the transpose of the selection matrix (made up of 0, 1 coefficients) which extracts edges of $\mathcal{G}_{\Gamma}$ from those of $\mathcal{G}_{\Omega_i}$. Coefficients of $\widetilde{\mathbf{h}}_{\Gamma}$ are mmfs computed along the edges of $\widetilde{\mathcal{G}}_{\Gamma}$ and are useful for coupling interior and exterior field problems. Coefficients of $\widetilde{\mathbf{j}}_{\Omega_i}$ are eddy currents in conductive parts only, since magnetic field sources are located in Ω_e.

The discrete magnetic diffusion equation is finally obtained in the same way as the corresponding local relationship (16). By letting (36) in (38) and (37) in (39), and by plugging constitutive relationships in (40), one obtains:

$$\left(\mathbf{C}_{\Omega_i}^{\mathrm{T}}\mathbf{M}_{\nu,\Omega_i}\mathbf{C}_{\Omega_i} + \imath\,\omega\,\mathbf{M}_{\sigma,\Omega_i}\right)\mathbf{a}_{\Omega_i} + \widetilde{\mathbf{C}}_{\Omega_i\Gamma}\,\widetilde{\mathbf{h}}_{\Gamma} = \mathbf{0}. \tag{41}$$

To couple interior and exterior field problems the interface term $\widetilde{\mathbf{a}}_{\Gamma}$ in (35), defined on the dual mesh, has to be mapped to the primal one as:

$$\widetilde{\mathbf{a}}_{\Gamma} = \mathbf{P}_{\Gamma}\,\widetilde{\mathbf{C}}_{\Omega_i\Gamma}^{\mathrm{T}}\,\mathbf{a}_{\Omega_i}, \tag{42}$$

where the projection matrix $\mathbf{P}_\Gamma$ is defined as discussed in [17], by using edge piecewise uniform basis functions, and $\widetilde{\mathbf{C}}^{\mathrm{T}}_{\Omega_i\Gamma}$ is the selection matrix which extracts edges of $\mathcal{G}_\Gamma$ from those of $\mathcal{G}_{\Omega_i}$. Similarly, $\widetilde{\mathbf{h}}_\Gamma$ in (41), defined on the dual mesh, can be derived from exterior DOFs as:

$$\widetilde{\mathbf{h}}_\Gamma = -\mathbf{P}_\Gamma\, \widetilde{\mathbf{C}}^{\mathrm{T}}_{\Omega_e\Gamma}\, \mathbf{h}_{\Omega_e}, \tag{43}$$

where the minus sign accounts for the opposite orientation of Γ and $\partial\Omega_e$. Finally, the interface magnetic fluxes in (31) can be expressed in terms of potentials as:

$$\widetilde{\mathbf{b}}_\Gamma = \widetilde{\mathbf{C}}_\Gamma\, \widetilde{\mathbf{a}}_\Gamma. \tag{44}$$

Note that (42) and (43) cannot be introduced in a FEM numerical scheme, based on a single cell complex only, which seems to motivate the inconsistencies in FEM numerical results observed by Kameari in [30].

In the a-φ electric formulation working variables are $\mathbf{a}_{\Omega_i}$, for the interior problem, and $\boldsymbol{\varphi}_{\Omega_e}, \boldsymbol{\xi}_{\Omega_e}$, for the exterior problem. By letting (42) in (35) and (43) in (41), and assembling together interior and exterior problem equations and topological constraints, a final symmetric linear system is obtained:

$$\begin{pmatrix} \mathbf{K}_{11} & \mathbf{K}_{12} & \mathbf{K}_{13} \\ \mathbf{K}_{21} & \mathbf{K}_{22} & \mathbf{O} \\ \mathbf{K}_{31} & \mathbf{O} & \mathbf{K}_{33} \end{pmatrix} \begin{pmatrix} \mathbf{a}_{\Omega_i} \\ \boldsymbol{\varphi}_{\Omega_e} \\ \boldsymbol{\xi}_{\Omega_e} \end{pmatrix} = \begin{pmatrix} \mathbf{f}_1 \\ \mathbf{f}_2 \\ \mathbf{f}_3 \end{pmatrix}, \tag{45}$$

where blocks of the upper triangular part are:

$$\begin{aligned}
\mathbf{K}_{11} &= \mathbf{C}^{\mathrm{T}}_{\Omega_i}\mathbf{M}_{\nu,\Omega_i}\mathbf{C}_{\Omega_i} + \imath\,\omega\,\mathbf{M}_{\sigma,\Omega_i}, \\
\mathbf{K}_{12} &= -\widetilde{\mathbf{C}}_{\Omega_i\Gamma}\,\mathbf{P}_\Gamma\,\widetilde{\mathbf{C}}^{\mathrm{T}}_{\Omega_e\Gamma}\,\mathbf{G}_{\Omega_e}, \\
\mathbf{K}_{13} &= -\widetilde{\mathbf{C}}_{\Omega_i\Gamma}\,\mathbf{P}_\Gamma\,\widetilde{\mathbf{C}}^{\mathrm{T}}_{\Omega_e\Gamma}\mathbf{T}_{\Omega_e}, \\
\mathbf{K}_{22} &= -\mathbf{G}^{\mathrm{T}}_{\Omega_e}\mathbf{M}_{\mu,\Omega_e}\mathbf{G}_{\Omega_e}, \\
\mathbf{K}_{33} &= -\mathbf{T}^{\mathrm{T}}_{\Omega_e}\mathbf{M}_{\mu,\Omega_e}\mathbf{T}_{\Omega_e},
\end{aligned}$$

and $\mathbf{K}_{21} = \mathbf{K}^{\mathrm{T}}_{12}$, $\mathbf{K}_{31} = \mathbf{K}^{\mathrm{T}}_{13}$ are the blocks in the lower triangular part, $\mathbf{O}$ is the null matrix. Vectors at the RHS are:

$$\begin{aligned}
\mathbf{f}_1 &= \widetilde{\mathbf{C}}_{\Omega_i\Gamma}\,\mathbf{P}_\Gamma\,\widetilde{\mathbf{C}}^{\mathrm{T}}_{\Omega_e\Gamma}\mathbf{h}_{0,\Omega_e}, \\
\mathbf{f}_2 &= \mathbf{G}^{\mathrm{T}}_{\Omega_e}\mathbf{M}_{\mu,\Omega_e}\mathbf{h}_{0,\Omega_e}, \\
\mathbf{f}_3 &= \mathbf{T}^{\mathrm{T}}_{\Omega_e}\mathbf{M}_{\mu,\Omega_e}\mathbf{h}_{0,\Omega_e}.
\end{aligned}$$

The final linear system is solved by using the transpose free quasi-minimal residual (TFQMR) iterative solver with symmetric successive over-relaxation (SSOR) preconditioner. Numerical tests showed that this solver has very good computational performance, low memory consumption, and smooth convergence pattern when solving (45).

By using the gauge transformation $\mathbf{a}_{\Omega_i} \mapsto \mathbf{a}_{\Omega_i} + \mathbf{G}_{\Omega_i}\mathbf{v}_{\Omega_i}$ in (41), where $\mathbf{v}_{\Omega_i}$ is the array of electric scalar potentials evaluated at the nodes of $\mathcal{G}_{\Omega_i}$, the alternative form of the magnetic diffusion equation is obtained:

$$\begin{aligned}
&\left(\mathbf{C}^{\mathrm{T}}_{\Omega_i}\mathbf{M}_{\nu,\Omega_i}\mathbf{C}_{\Omega_i} + \imath\,\omega\,\mathbf{M}_{\sigma,\Omega_i}\right)\mathbf{a}_{\Omega_i} \\
&\qquad + \imath\,\omega\,\mathbf{M}_{\sigma,\Omega_i}\mathbf{G}_{\Omega_i}\mathbf{v}_{\Omega_i} + \widetilde{\mathbf{C}}_{\Omega_i\Gamma}\,\widetilde{\mathbf{h}}_\Gamma = \mathbf{0}
\end{aligned} \tag{46}$$

which corresponds to (17) at the discrete level. Coefficients of $\mathbf{v}_{\Omega_i}$ are non-zero only in correspondence of the nodes of $\mathcal{G}_{\Omega_C}$.

By integrating (6) on each cell of $\widetilde{\mathcal{G}}_{\Omega_i}$ the electric conservation equation at the discrete level becomes:

$$\widetilde{\mathbf{D}}_{\Omega_i}\,\widetilde{\mathbf{j}}_{\Omega_i} = \mathbf{0}, \tag{47}$$

where $\widetilde{\mathbf{D}}_{\Omega_i} = -\mathbf{G}^{\mathrm{T}}_{\Omega_i}$ is the cell-to-face incidence matrix of $\widetilde{\mathcal{G}}_{\Omega_i}$ and $\widetilde{\mathbf{j}}_{\Omega_i}$ is the array of currents through the faces of $\widetilde{\mathcal{G}}_{\Omega_i}$. By using the gauge transformation in (36), emfs along the edges of $\mathcal{G}_{\Omega_i}$ can be expressed as:

$$\mathbf{e}_{\Omega_i} = -\imath\,\omega\,\left(\mathbf{a}_{\Omega_i} + \mathbf{G}_{\Omega_i}\mathbf{v}_{\Omega_i}\right). \tag{48}$$

By letting (38) in (47) and by using (48), one obtains:

$$\imath\,\omega\,\mathbf{G}^{\mathrm{T}}_{\Omega_i}\mathbf{M}_{\sigma,\Omega_i}\mathbf{a}_{\Omega_i} + \imath\,\omega\,\mathbf{G}^{\mathrm{T}}_{\Omega_i}\mathbf{M}_{\sigma,\Omega_i}\mathbf{G}_{\Omega_i}\mathbf{v}_{\Omega_i} = \mathbf{0}, \tag{49}$$

which corresponds to (18) at the discrete level.

The final matrix of the a, v-φ formulation is obtained in the same way as (45), with the only difference that (41) is used instead of (46). Moreover, additional constraints for electric scalar potentials, provided in (49), are required. The following symmetric linear system is obtained:

$$\begin{pmatrix} \mathbf{K}_{11} & \mathbf{K}_{12} & \mathbf{K}_{13} & \mathbf{K}_{14} \\ \mathbf{K}_{21} & \mathbf{K}_{22} & \mathbf{O} & \mathbf{O} \\ \mathbf{K}_{31} & \mathbf{O} & \mathbf{K}_{33} & \mathbf{O} \\ \mathbf{K}_{41} & \mathbf{O} & \mathbf{O} & \mathbf{K}_{44} \end{pmatrix} \begin{pmatrix} \mathbf{a}_{\Omega_i} \\ \mathbf{v}_{\Omega_i} \\ \boldsymbol{\varphi}_{\Omega_e} \\ \boldsymbol{\xi}_{\Omega_e} \end{pmatrix} = \begin{pmatrix} \mathbf{f}_1 \\ \mathbf{0} \\ \mathbf{f}_3 \\ \mathbf{f}_4 \end{pmatrix}, \tag{50}$$

where blocks of the upper triangular part are:

$$\begin{aligned}
\mathbf{K}_{11} &= \mathbf{C}^{\mathrm{T}}_{\Omega_i}\mathbf{M}_{\nu,\Omega_i}\mathbf{C}_{\Omega_i} + \imath\,\omega\,\mathbf{M}_{\sigma,\Omega_i}, \\
\mathbf{K}_{12} &= \imath\,\omega\,\mathbf{M}_{\sigma,\Omega_i}\mathbf{G}_{\Omega_i}, \\
\mathbf{K}_{13} &= -\widetilde{\mathbf{C}}_{\Omega_i\Gamma}\,\mathbf{P}_\Gamma\,\widetilde{\mathbf{C}}^{\mathrm{T}}_{\Omega_e\Gamma}\,\mathbf{G}_{\Omega_e}, \\
\mathbf{K}_{14} &= -\widetilde{\mathbf{C}}_{\Omega_i\Gamma}\,\mathbf{P}_\Gamma\,\widetilde{\mathbf{C}}^{\mathrm{T}}_{\Omega_e\Gamma}\mathbf{T}_{\Omega_e}, \\
\mathbf{K}_{22} &= \imath\,\omega\,\mathbf{G}^{\mathrm{T}}_{\Omega_i}\mathbf{M}_{\sigma,\Omega_i}\mathbf{G}_{\Omega_i}, \\
\mathbf{K}_{33} &= -\mathbf{G}^{\mathrm{T}}_{\Omega_e}\mathbf{M}_{\mu,\Omega_e}\mathbf{G}_{\Omega_e}, \\
\mathbf{K}_{44} &= -\mathbf{T}^{\mathrm{T}}_{\Omega_e}\mathbf{M}_{\mu,\Omega_e}\mathbf{T}_{\Omega_e},
\end{aligned}$$

and $\mathbf{K}_{21} = \mathbf{K}^{\mathrm{T}}_{12}$, $\mathbf{K}_{31} = \mathbf{K}^{\mathrm{T}}_{13}$, $\mathbf{K}_{41} = \mathbf{K}^{\mathrm{T}}_{14}$ are the blocks in the lower triangular part. Vectors at the RHS are:

$$\begin{aligned}
\mathbf{f}_1 &= \widetilde{\mathbf{C}}_{\Omega_i\Gamma}\,\mathbf{P}_\Gamma\,\widetilde{\mathbf{C}}^{\mathrm{T}}_{\Omega_e\Gamma}\mathbf{h}_{0,\Omega_e}, \\
\mathbf{f}_3 &= \mathbf{G}^{\mathrm{T}}_{\Omega_e}\mathbf{M}_{\mu,\Omega_e}\mathbf{h}_{0,\Omega_e}, \\
\mathbf{f}_4 &= \mathbf{T}^{\mathrm{T}}_{\Omega_e}\mathbf{M}_{\mu,\Omega_e}\mathbf{h}_{0,\Omega_e}.
\end{aligned}$$

The final linear system of the a, v-φ formulation is solved by using the same TFQMR+SSOR iterative solver as above.

D. MAGNETIC HYBRID FORMULATIONS

By integrating (1) on the faces of $\widetilde{\mathcal{G}}_{\Omega_i}$ and by applying Stokes' theorem, the discrete Faraday's law reads:

$$\widetilde{\mathbf{C}}_{\Omega_i}\widetilde{\mathbf{e}}_{\Omega_i} + \widetilde{\mathbf{C}}_{\Omega_i\Gamma}\,\widetilde{\mathbf{e}}_\Gamma = -\imath\,\omega\,\widetilde{\mathbf{b}}_{\Omega_i}, \tag{51}$$

where $\widetilde{\mathbf{e}}_{\Omega_i}$, $\widetilde{\mathbf{e}}_\Gamma$ are the arrays of emfs along the edges of $\widetilde{\mathcal{G}}_{\Omega_i}$ and $\widetilde{\mathcal{G}}_\Gamma$, respectively, and $\widetilde{\mathbf{b}}_{\Omega_i}$ is the array of magnetic fluxes through the faces of $\widetilde{\mathcal{G}}_{\Omega_i}$. By approximating local relationships (19) and (12) with piecewise uniform bases, the electric and magnetic constitutive relationships become:

$$\widetilde{\mathbf{e}}_{\Omega_i} = \mathbf{M}_{\rho,\Omega_i}\,\mathbf{j}_{\Omega_i}, \tag{52}$$

$$\widetilde{\mathbf{b}}_{\Omega_i} = \mathbf{M}_{\mu,\Omega_i}\,\mathbf{h}_{\Omega_i}, \tag{53}$$

where $\mathbf{j}_{\Omega_i}$ is the array of currents through the faces of $\mathcal{G}_{\Omega_i}$ and $\mathbf{h}_{\Omega_i}$ is the array of mmfs along the edges of $\mathcal{G}_{\Omega_i}$. The resistance $\mathbf{M}_{\rho,\Omega_i}$ and the inductance matrix $\mathbf{M}_{\mu,\Omega_i}$ are computed in the same way as $\mathbf{M}_{\nu,\Omega_i}$ and $\mathbf{M}_{\sigma,\Omega_i}$, respectively. By integrating (2) on the faces of $\mathcal{G}_{\Omega_i}$ and by applying Stokes' theorem, Ampére's law in the interior region reads:

$$\mathbf{C}_{\Omega_i}\mathbf{h}_{\Omega_i} = \mathbf{j}_{\Omega_i}. \tag{54}$$

By letting constitutive relationships (52) and (32) in (51), and by using (54), the discrete magnetic diffusion equation reads:

$$\left(\mathbf{C}_{\Omega_i}^{\mathrm{T}}\mathbf{M}_{\mu,\Omega_i}\mathbf{C}_{\Omega_i} + \imath\,\omega\,\mathbf{M}_{\mu,\Omega_i}\right)\mathbf{h}_{\Omega_i} + \widetilde{\mathbf{C}}_{\Omega_i\Gamma}\,\widetilde{\mathbf{e}}_{\Gamma} = \mathbf{0}. \tag{55}$$

To couple interior and exterior problems interface terms in (33) and (35) need to be expressed in terms of emfs $\widetilde{\mathbf{e}}_{\Gamma}$ by using these equivalent forms of Faraday's law:

$$\widetilde{\mathbf{a}}_{\Gamma} = -\imath\,\omega^{-1}\,\widetilde{\mathbf{e}}_{\Gamma}, \tag{56}$$
$$\widetilde{\mathbf{b}}_{\Gamma} = \imath\,\omega^{-1}\,\widetilde{\mathbf{C}}_{\Gamma}\,\widetilde{\mathbf{e}}_{\Gamma}, \tag{57}$$

where $\widetilde{\mathbf{C}}_{\Gamma}$ is the face-to-edge incidence matrix of $\widetilde{\mathcal{G}}_{\Gamma}$. Emfs need to be constrained by an additional set of equations, which fulfill the continuity of mmfs across the interface. By integrating (9) along the edges of $\mathcal{G}_{\Gamma}$, one obtains:

$$\mathbf{h}_{\Gamma} = \mathbf{h}_{0,\Gamma} + \mathbf{G}_{\Gamma}\,\boldsymbol{\varphi}_{\Gamma} + \sum_{k=1}^{\beta_1}\xi_k\,\mathbf{t}_{k,\Gamma}, \tag{58}$$

where coefficients of interface arrays can be extracted from bulk ones by means of selection matrices as $\mathbf{h}_{\Gamma} = \widetilde{\mathbf{C}}_{\Omega_i\Gamma}^{\mathrm{T}}\mathbf{h}_{\Omega_i}$, $\mathbf{h}_{0,\Gamma} = \widetilde{\mathbf{C}}_{\Omega_i\Gamma}^{\mathrm{T}}\mathbf{h}_{0,\Omega_i}$, $\boldsymbol{\varphi}_{\Gamma} = \widetilde{\mathbf{D}}_{\Omega_i\Gamma}^{\mathrm{T}}\boldsymbol{\varphi}_{\Omega_i}$, $\mathbf{t}_{k,\Gamma} = \widetilde{\mathbf{C}}_{\Omega_i\Gamma}^{\mathrm{T}}\mathbf{t}_{k,\Omega_i}$.

In the h-φ electric formulation working variables are $\mathbf{h}_{\Omega_i}$, for the interior problem, and $\boldsymbol{\varphi}_{\Omega_e}$, $\boldsymbol{\xi}_{\Omega_e}$, for the exterior problem. By assembling the magnetic diffusion equation (46), the magnetostatic equations (33), topological constraints (35), and the additional constraint for emfs (58), the following symmetric linear system is obtained:

$$\begin{pmatrix} \mathbf{K}_{11} & \mathbf{O} & \mathbf{O} & \mathbf{K}_{14} \\ \mathbf{O} & \mathbf{K}_{22} & \mathbf{O} & \mathbf{K}_{24} \\ \mathbf{O} & \mathbf{O} & \mathbf{K}_{33} & \mathbf{K}_{34} \\ \mathbf{K}_{41} & \mathbf{K}_{42} & \mathbf{K}_{43} & \mathbf{O} \end{pmatrix} \begin{pmatrix} \mathbf{h}_{\Omega_i} \\ \boldsymbol{\varphi}_{\Omega_e} \\ \boldsymbol{\xi}_{\Omega_e} \\ \widetilde{\mathbf{e}}_{\Gamma} \end{pmatrix} = \begin{pmatrix} \mathbf{0} \\ \mathbf{f}_2 \\ \mathbf{f}_3 \\ \mathbf{f}_4 \end{pmatrix}, \tag{59}$$

where blocks of the upper triangular part are:

$$\begin{aligned}
\mathbf{K}_{11} &= \mathbf{C}_{\Omega_i}^{\mathrm{T}}\mathbf{M}_{\rho,\Omega_i}\mathbf{C}_{\Omega_i} + \imath\,\omega\,\mathbf{M}_{\mu,\Omega_i},\\
\mathbf{K}_{14} &= \widetilde{\mathbf{C}}_{\Omega_i\Gamma},\\
\mathbf{K}_{22} &= \imath\,\omega\,\mathbf{G}_{\Omega_e}^{\mathrm{T}}\mathbf{M}_{\mu,\Omega_e}\mathbf{G}_{\Omega_e},\\
\mathbf{K}_{24} &= \widetilde{\mathbf{D}}_{\Omega_e\Gamma}\,\widetilde{\mathbf{C}}_{\Gamma},\\
\mathbf{K}_{33} &= \imath\,\omega\,\mathbf{T}_{\Omega_e}^{\mathrm{T}}\mathbf{M}_{\mu,\Omega_e}\mathbf{T}_{\Omega_e},\\
\mathbf{K}_{34} &= -\mathbf{T}_{\Omega_e}^{\mathrm{T}}\widetilde{\mathbf{C}}_{\Omega_e\Gamma},
\end{aligned}$$

and $\mathbf{K}_{41} = \mathbf{K}_{14}^{\mathrm{T}}$, $\mathbf{K}_{42} = \mathbf{K}_{24}^{\mathrm{T}}$, $\mathbf{K}_{43} = \mathbf{K}_{34}^{\mathrm{T}}$ are the blocks in the lower triangular part. Vectors at the RHS are:

$$\begin{aligned}
\mathbf{f}_2 &= -\imath\,\omega\,\mathbf{G}_{\Omega_e}^{\mathrm{T}}\mathbf{M}_{\mu,\Omega_e}\mathbf{h}_{0,\Omega_e},\\
\mathbf{f}_3 &= -\imath\,\omega\,\mathbf{T}_{\Omega_e}^{\mathrm{T}}\mathbf{M}_{\mu,\Omega_e}\mathbf{h}_{0,\Omega_e},\\
\mathbf{f}_4 &= \widetilde{\mathbf{C}}_{\Omega_e\Gamma}^{\mathrm{T}}\mathbf{h}_{0,\Omega_e}.
\end{aligned}$$

The final linear system results to be in a saddle-point form, which is not suitable for an efficient solution. Therefore, emfs are eliminated by the numerical strategy proposed in [16]. After reduction, (59) can be solved by using the TFQMR + SSOR iterative solver adopted above.

By using the gauge transformation $\mathbf{h}_{\Omega_i} \mapsto \mathbf{t}_{\Omega_i} + \mathbf{G}_{\Omega_i}\boldsymbol{\varphi}_{\Omega_i}$ in (55), where $\boldsymbol{\varphi}_{\Omega_i}$ is the array of magnetic scalar potentials evaluated at the nodes of $\mathcal{G}_{\Omega_i}$, the alternative form of the magnetic diffusion equation is obtained:

$$\begin{aligned}
\left(\mathbf{C}_{\Omega_i}^{\mathrm{T}}\mathbf{M}_{\rho,\Omega_i}\mathbf{C}_{\Omega_i} + \imath\,\omega\,\mathbf{M}_{\mu,\Omega_i}\right)\mathbf{t}_{\Omega_i}&\\
+\imath\,\omega\,\mathbf{M}_{\mu,\Omega_i}\mathbf{G}_{\Omega_i}\boldsymbol{\varphi}_{\Omega_i} + \widetilde{\mathbf{C}}_{\Omega_i\Gamma}\,\widetilde{\mathbf{e}}_{\Gamma} &= \mathbf{0},
\end{aligned} \tag{60}$$

which corresponds to (21) at the discrete level. By integrating (5) on each cell of $\widetilde{\mathcal{G}}_{\Omega_i}$ the magnetic conservation equation in the interior region is obtained:

$$\widetilde{\mathbf{D}}_{\Omega_i}\,\widetilde{\mathbf{b}}_{\Omega_i} + \widetilde{\mathbf{D}}_{\Omega_i\Gamma}\,\widetilde{\mathbf{b}}_{\Gamma} = \mathbf{0}, \tag{61}$$

where magnetic fluxes in the bulk domain can be expressed in terms of mmfs by using the constitutive relationship:

$$\widetilde{\mathbf{b}}_{\Omega_i} = \mathbf{M}_{\mu,\Omega_i}\,\mathbf{h}_{\Omega_i}. \tag{62}$$

By inserting (62) in (61), with $\widetilde{\mathbf{D}}_{\Omega_i} = -\mathbf{G}_{\Omega_i}^{\mathrm{T}}$, and by using the gauge transformation, one obtains:

$$\mathbf{G}_{\Omega_i}^{\mathrm{T}}\mathbf{M}_{\mu,\Omega_i}\mathbf{t}_{\Omega_i} + \mathbf{G}_{\Omega_i}^{\mathrm{T}}\mathbf{M}_{\mu,\Omega_i}\mathbf{G}_{\Omega_i}\boldsymbol{\varphi}_{\Omega_i} - \widetilde{\mathbf{D}}_{\Omega_i\Gamma}\widetilde{\mathbf{b}}_{\Gamma} = \mathbf{0}. \tag{63}$$

Potentials in the interior and exterior region can be extracted from potentials evaluated at the nodes of the whole mesh as:

$$\boldsymbol{\varphi}_{\Omega_i} = \mathbf{Q}_{\Omega_i}\boldsymbol{\varphi}_{\Omega}, \tag{64}$$
$$\boldsymbol{\varphi}_{\Omega_e} = \mathbf{Q}_{\Omega_e}\boldsymbol{\varphi}_{\Omega}, \tag{65}$$

where $\mathbf{Q}_{\Omega_i}$ and $\mathbf{Q}_{\Omega_e}$ are selection matrices made of 0, 1 coefficients, which extract potentials related to nodes of $\mathcal{G}_{\Omega_i}$ and $\mathcal{G}_{\Omega_e}$ from those of $\mathcal{G}_{\Omega}$, respectively.

The magnetic flux conservation equation in the whole computational domain can be obtained by assembling the corresponding equations of interior and exterior regions. This assembly can be carried out by left multiplying (33) and (63) by $\mathbf{Q}_e^{\mathrm{T}}$ and $\mathbf{Q}_i^{\mathrm{T}}$, respectively. By using positions (64) and (65), one obtains the conservation relationship over $\mathcal{G}_{\Omega}$:

$$\begin{aligned}
\mathbf{Q}_i^{\mathrm{T}}\mathbf{G}_{\Omega_i}^{\mathrm{T}}\mathbf{M}_{\mu,\Omega_i}\mathbf{t}_{\Omega_i} + \mathbf{G}_{\Omega}^{\mathrm{T}}\,\mathbf{M}_{\mu,\Omega}\,\mathbf{G}_{\Omega}\,\boldsymbol{\varphi}_{\Omega}&\\
= -\mathbf{Q}_e^{\mathrm{T}}\,\mathbf{G}_{\Omega_e}^{\mathrm{T}}\mathbf{M}_{\mu,\Omega_e}\mathbf{h}_{0,\Omega_e},&
\end{aligned} \tag{66}$$

where $\mathbf{G}_{\Omega}$ and $\mathbf{M}_{\mu,\Omega}$ are assembled from corresponding matrices of $\mathcal{G}_{\Omega_i}$ and $\mathcal{G}_{\Omega_e}$. It has to be noted that interface terms in (33) and (63) cancel out when assembling, due to the opposite orientation of $\partial\Omega_i$ and $\partial\Omega_e$.

The final linear system of the t–φ formulation is obtained by assembling the magnetic diffusion equation (60), the

global magnetic flux conservation (66), topological constraints (35), and the additional constraint for emfs (58). The following symmetric linear system is obtained:

$$\begin{pmatrix} \mathbf{K}_{11} & \mathbf{K}_{12} & \mathbf{O} & \mathbf{K}_{14} \\ \mathbf{K}_{21} & \mathbf{K}_{22} & \mathbf{O} & \mathbf{O} \\ \mathbf{O} & \mathbf{O} & \mathbf{K}_{33} & \mathbf{K}_{34} \\ \mathbf{K}_{41} & \mathbf{O} & \mathbf{K}_{43} & \mathbf{O} \end{pmatrix} \begin{pmatrix} \mathbf{t}_{\Omega_i} \\ \boldsymbol{\varphi}_{\Omega} \\ \boldsymbol{\xi}_{\Omega_e} \\ \widetilde{\mathbf{e}}_{\Gamma} \end{pmatrix} = \begin{pmatrix} \mathbf{0} \\ \mathbf{f}_2 \\ \mathbf{f}_3 \\ \mathbf{f}_4 \end{pmatrix}, \quad (67)$$

where blocks of the upper triangular part are:

$$\begin{aligned} \mathbf{K}_{11} &= \mathbf{C}_{\Omega_i}^{\mathrm{T}} \mathbf{M}_{\rho,\Omega_i} \mathbf{C}_{\Omega_i} + \imath\, \omega\, \mathbf{M}_{\mu,\Omega_i}, \\ \mathbf{K}_{12} &= \imath\, \omega\, \mathbf{M}_{\mu,\Omega_i} \mathbf{G}_{\Omega_i} \mathbf{Q}_{\Omega_i}, \\ \mathbf{K}_{14} &= \widetilde{\mathbf{C}}_{\Omega_i\Gamma}, \\ \mathbf{K}_{22} &= \imath\, \omega\, \mathbf{G}_{\Omega}^{\mathrm{T}} \mathbf{M}_{\mu,\Omega} \mathbf{G}_{\Omega}, \\ \mathbf{K}_{33} &= \imath\, \omega\, \mathbf{T}_{\Omega_e}^{\mathrm{T}} \mathbf{M}_{\mu,\Omega_e} \mathbf{T}_{\Omega_e}, \\ \mathbf{K}_{34} &= -\mathbf{T}_{\Omega_e}^{\mathrm{T}} \widetilde{\mathbf{C}}_{\Omega_e\Gamma}, \end{aligned}$$

and $\mathbf{K}_{21} = \mathbf{K}_{12}^{\mathrm{T}}$, $\mathbf{K}_{41} = \mathbf{K}_{14}^{\mathrm{T}}$, $\mathbf{K}_{43} = \mathbf{K}_{34}^{\mathrm{T}}$ are the blocks in the lower triangular part. Vectors at the RHS are:

$$\begin{aligned} \mathbf{f}_2 &= -\imath\, \omega\, \mathbf{Q}_{\Omega_e}^{\mathrm{T}} \mathbf{G}_{\Omega_e}^{\mathrm{T}} \mathbf{M}_{\mu,\Omega_e} \mathbf{h}_{0,\Omega_e}, \\ \mathbf{f}_3 &= -\imath\, \omega\, \mathbf{T}_{\Omega_e}^{\mathrm{T}} \mathbf{M}_{\mu,\Omega_e} \mathbf{h}_{0,\Omega_e}, \\ \mathbf{f}_4 &= \widetilde{\mathbf{C}}_{\Omega_e\Gamma}^{\mathrm{T}} \mathbf{h}_{0,\Omega_e}. \end{aligned}$$

Emfs are eliminated from (67) in a similar fashion as h-φ formulation to allow for a fast TFQMR+SSOR solution.

V. NUMERICAL RESULTS

The multigrid-based algorithm for finding cohomology, presented in Section III, and hybrid formulations, presented in Section IV, were implemented in MATLAB® software. Functions for matrix assembly in particular were implemented in a vectorized-language style to run real-size models of a few millions DOFs at limited cost. All numerical tests were run on a laptop with an Intel Core i7-6920HQ processor (8 MB cache, 2.9 GHz frequency), 16 GB RAM.

Hybrid formulations were tested on two benchmarks, i.e., the so-called ''Bath plate'' model (Team problem no. 3) of the International Compumag Society [31] and the toroidal transformer model. The first benchmark is a well-know model for testing numerical methods for multiply connected eddy-current problems (see, e.g., [32]) and consists in a conductive plate with two holes excited by an AC current-driven coil. The second benchmark consists in a toroidal solenoid excited by an AC current loop located along the solenoid axis. It represents an example of model topology for which cohomology cannot be computed by Gmsh software in a reasonable time, due to algebraic computations with large integer matrices.

The computing performance of the multigrid-based algorithm was compared with that of the Gmsh algorithm, based on homological algebra, described in [14]. Main steps for computing cohomology in Gmsh can be summarized as:

1) First, volumes-to-faces, faces-to-edges, and edges-to-nodes incidence matrices of the mesh are constructed or, equivalently, the oriented boundary relations of the mesh elements are enumerated. The computational complexity of this step is $\mathcal{O}(N \log N)$.
2) Second, incidence matrices are reduced so that the cohomology groups they induce remain equivalent. This amounts to reducing the original finite element mesh, removing and combining its elements [13]. Reduction algorithms are usually able to reduce the mesh to a tiny fraction of the original one, resulting in incidence matrices of small size as it results in the case of Bath plate benchmark. However, the toroidal transformer benchmark is a counter-example where the reduction algorithms are inefficient. Their computational complexity ranges from $\mathcal{O}(N \log N)$ to $\mathcal{O}(N^2)$. They are applied in succession so that most of the work is carried out by algorithms with lowest complexity.
3) Finally, the first cohomology group is computed from the transpose of the faces-to-edges incidence matrix by using the SNF integer matrix decomposition in three different group algebraic subproblems, with $\mathcal{O}(N^3)$ computational complexity. Each cohomology generator computed on the reduced mesh is represented as a set of edges in the original mesh, each one associated to an integer coefficient.

A. BATH PLATE BENCHMARK

The Bath Plate problem consists in a conducting plate (32.78 MS/m conductivity, $\mu_r = 1$ relative permeability) of $60 \times 110 \times 6.35$ mm size and two symmetric holes of 40×30 mm size (Fig. 2). In such a way the conductive region is multiply connected, with $\beta_1 = 2$. The whole model is embedded into a cube of 2 m side to exclude boundary effects on field calculations. The origin of the Cartesian reference frame (x, y, z) is centered on the plate surface; distances are all expressed in millimeters. The conductor is excited by a cylindrical coil (20×20 mm cross-section, 1240 A RMS current) centered at $(0, 0, 25)$. Two different current frequency values are adopted: 50 Hz, 200 Hz. Line in Fig. 2 goes from point A $(0, -55, 0.5)$ to B $(0, 55, 0.5)$ and it is used for comparing the magnetic flux density. Moreover, global quantities are evaluated through cuts shown in Fig. 3.

The Bath Plate model was discretized by using different mesh refinements in order to assess the computing performance of AGMGccc solver (used to obtained the source field in (30)), and that of Algorithm 1, based again on AGMGcc. All tetrahedral meshes were generated by using a commercial finite element software and then imported in MATLAB® environment for processing with in-house software implementing hybrid formulations.

The source field was first computed as described in Section IV-A to represent the effect of current-driven coil on the solution. Table 1 shows the CPU time needed for solving the curl-curl linear system (30) by AGMGcc solver. It can be observed that AGMGcc exhibits a constant number of iterations for different mesh sizes, thus showing $\mathcal{O}(N)$ complexity. Moreover, CPU time turns out to be limited

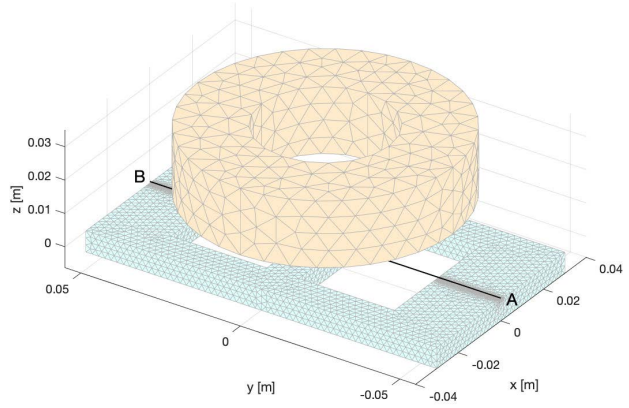

FIGURE 2. Team problem 3: An aluminum plate with two holes ($\beta_1 = 2$) is excited by a current driven coil at two different frequencies (50, 200 Hz). Magnetic flux density is computed 0.5 mm above the plate surface along line AB.

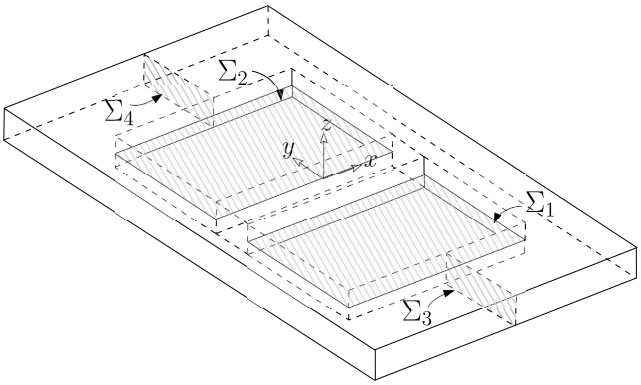

FIGURE 3. Cuts for computing magnetic flux (Σ_1, Σ_2) and for computing eddy current (Σ_3, Σ_4) of Team 3 benchmark.

TABLE 1. Computational performance of source field generation for different meshes. (Team 3.)

# tets	CPU time (s) (solution)	AGMGcc # DOFs	AGMGcc # iterations
293 051	2.52	344 427	17
1 026 097	8.30	1 210 887	17
2 033 776	16.18	2 396 116	17
3 376 375	27.91	3 972 105	17

(i.e., a few tens of seconds) even with meshes comprising a few million elements.

The computational performance of Algorithm 1 described in Section III was compared with that of Gmsh software by considering the same mesh refinements as above. The Bath Plate model was implemented also in Gmsh and meshes of comparable sizes were generated to compute cohomology by Gmsh. It can be observed in Fig. 4 that the multigrid-based

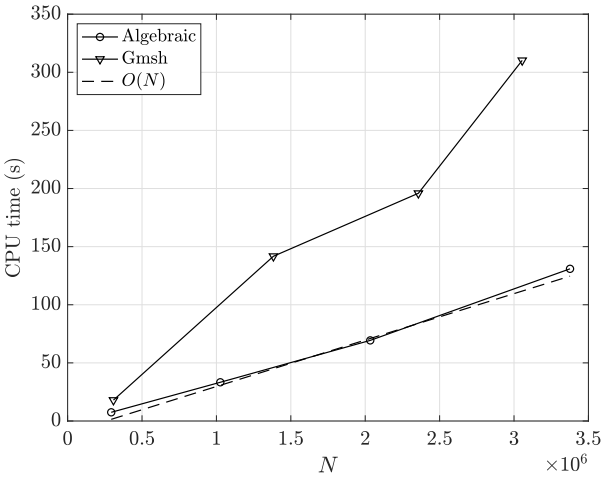

FIGURE 4. Computational time-complexity of multigrid-based algorithm and Gmsh software: CPU time (s) vs. number of tetrahedrons N. (Team 3.)

TABLE 2. Computational performance of multigrid-based algorithm for different meshes. (Team 3.)

# tets	CPU time (s) (generation)	AGMGcc # DOFs	AGMGcc # iterations	
			$k = 1$	$k = 2$
293 051	7.48	280 822	31	25
1 026 097	33.31	1 147 245	35	24
2 033 776	69.35	2 332 474	34	25
3 376 375	130.92	3 908 463	37	28

algorithm has optimal computational complexity, whereas computing cost is super-linear in the case of Gmsh. In particular, for a mesh of a few million elements the CPU time of Gmsh algorithm is about three times than that of multigrid-based algorithm. Table 2 shows that cohomology is computed by multigrid-based algorithm in a few tens of seconds even for curl-curl linear systems of a few million elements. The cost of AGMGcc solver in Algorithm 1 is predominant with respect to that of AGMG solver; therefore only the number of DOFs of AGMGcc is considered in Table 2. For both solvers the relative tolerance is fixed to 10^{-10}. It can be observed that the number of AGMGcc iterations needed to compute the second generator ($k = 2$) is about 30% less than those needed to compute the first generator ($k = 1$). In fact the trial solution for AGMGcc solver is updated at any while loop with the last computed solution. Moreover, preconditioner in Algorithm 1 is set up only once to further speed up the solution.

Once source field and cohomology generators have been computed, the final linear system is obtained. Numerical tests considered in the following are based on the same discretized model with 293 051 tetrahedrons (60 832 of which are used

TABLE 3. Computational performance of hybrid methods for the coarsest mesh in Table 1. (Team 3, 50 Hz.)

method	CPU time (s) (assembly)	CPU time (s) (solution)	TFQMR # DOFs	TFQMR # iterations
a-φ	17.73	33.41	120 634	1125
a, v-φ	18.40	15.31	133 436	333
h-φ	19.18	36.47	105 586	1309
t-φ	19.07	4.80	113 374	127

TABLE 4. Computational performance of hybrid methods for the coarsest mesh in Table 1. (Team 3, 200 Hz.)

method	CPU time (s) (assembly)	CPU time (s) (solution)	TFQMR # DOFs	TFQMR # iterations
a-φ	18.10	25.63	120 634	863
a, v-φ	19.67	13.42	133 436	262
h-φ	18.30	23.27	105 586	856
t-φ	18.10	5.72	113 374	152

to mesh the conductive domain in order to capture the skin effect inside the plate at 200 Hz). This corresponds to the coarsest mesh refinement in previous complexity analyses. All four different formulations can be solved with the same numerical strategy based on TFMR solver with SSOR preconditioner since final symmetric systems show the same algebraic properties, being complex, symmetric, indefinite, and sparse. It has to be noted that electric hybrid formulations do not need a preliminary linear system reduction, which is however carried out at negligible computing cost in magnetic hybrid formulations by fast matrix-vector multiplications in MATLAB®.

The computational performance of different hybrid formulations was compared at 50 and 200 Hz in Table 3 and 4. The assembly time includes the computation of both source field and cohomology generators, and that of matrix blocks and RHS vectors of the final linear systems. It can be observed that the assembly time is basically the same for all hybrid formulations. The introduction of electric scalar potential in the a, v-φ formulation and the extension of the magnetic scalar potential to the whole domain in the t-φ formulation allow for a considerable reduction of TFQMR solver iterations, compared to a-φ and h-φ formulations proposed in [16] and [17], respectively. In particular, t-φ formulation shows an outstanding numerical performance with a CPU time for linear system solution of a few seconds, which is one eight of solution time of a-φ and h-φ formulations at 50 Hz. Similar results can be observed at 200 Hz. The minimum amount of DOFs for representing the eddy current problem is needed by the h-φ formulation, in which interface edge variables are eliminated during the solution process.

Fig. 5 and 6 show that all formulations exhibit a smooth convergence pattern. In particular, the t-φ formulation attains in 127 iterations 10^{-10} relative tolerance. Fig. 6 shows that the convergence behavior of t-φ formulation is almost independent of frequency. Only a small change of the convergence pattern is observed in Fig. 5 for the a, v-φ formulation.

To verify the accuracy of proposed numerical methods, the z–component of the magnetic flux density (real and imaginary parts) was computed in 401 equally spaced points along the line AB in Fig. 2. The reference solution was obtained by

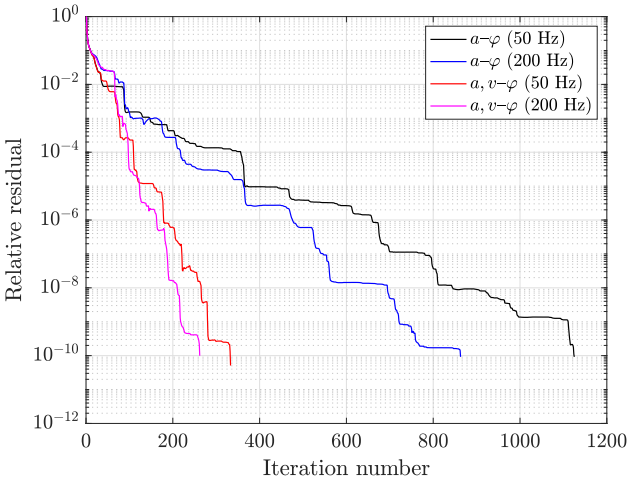

FIGURE 5. Convergence pattern of TFQMR solver for electric formulations at 50, 200 Hz frequency. (Team 3.)

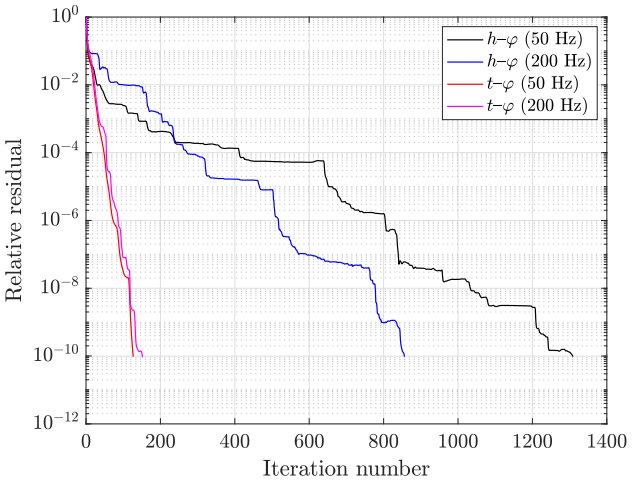

FIGURE 6. Convergence pattern of TFQMR solver for magnetic formulations at 50, 200 Hz frequency. (Team 3.)

using a commercial finite-element software implementing the classical A, V-A formulation with second-order tetrahedrons. The FEM linear system (with 1 169 002 DOFs) was solved by TFQMR with geometric multigrid preconditioner, with the same tolerance as above. To reduce the amount of DOFs,

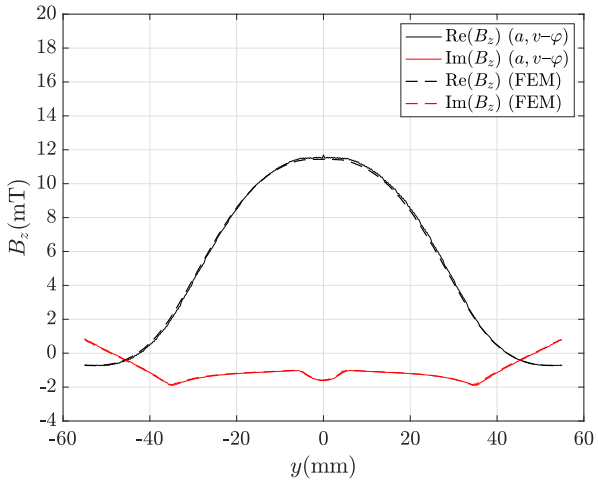

FIGURE 7. Real and imaginary parts of the magnetic flux density (z-axis component) computed along the line AB in Fig. 2 by using the a, v-φ formulation.

and thus memory requirements, in this case only half-model was considered by exploiting symmetry. The solver attained 10^{-10} relative tolerance in 163 s at 50 Hz. In order to stabilize the FEM solver a fake conductance (1 S/m) had to be adopted in the air region, which may slightly affect the solution accuracy. This fake conductance is not required by the proposed methods since they make use of separate discretization variables for interior and exterior regions. Fig. 7 shows that the real and imaginary parts of the magnetic flux density z–component of the a, v-φ formulation at 50 Hz are in very good agreement with the corresponding field profiles obtained by second-order FEM. In this case the maximum discrepancy is 2.23% for the real part and 4.80% for the imaginary part. Comparable levels of accuracy were obtained by considering the other hybrid formulations and by increasing the frequency up to 200 Hz. It has to be noted that numerical results of hybrid formulations are accurate, although much fewer degrees of freedom than those used in the FEM model. Solution time of all four formulations is also negligible compared to the FEM one.

The accuracy of the proposed formulations was assessed also by comparing global quantities such as magnetic fluxes and eddy current through cuts. In Fig. 3, cuts Σ_1 and Σ_2, with dimensions 40 × 30 mm, are obtained by cutting holes in the air region at $z = -3$ mm. Σ_3 and Σ_4, with dimensions 20 × 6.35 mm, are the intersections of the plate and the vertical plane $x = 0$. Magnetic fluxes Φ_1, Φ_2 computed through Σ_1, Σ_2 by second-order FEM (as a reference) and hybrid formulations are reported in Table 5 (50 Hz) and 6 (200 Hz). Due to model symmetry, relationship $\Phi_1 = \Phi_2$ theoretically holds. All formulations show limited discrepancy between Φ_1 and Φ_2. It can be noted that t-φ formulation shows the best agreement with FEM at 50 Hz and electric formulations provide the same level of accuracy.

The same comparisons as above were carried out by considering eddy currents I_3, I_4 through Σ_3, Σ_4. Due to the model symmetry, relationship $I_3 = -I_4$ theoretically holds. Table 7 (at 50 Hz) and Table 8 (at 200 Hz) show that this condition is well approximated by all hybrid formulations. The best agreement with second-order FEM is attained by t-φ formulation at 50 Hz and by a-φ formulation at 200 Hz.

TABLE 5. Magnetic flux through (μ T) cuts Σ_1, Σ_2 in Fig. 3 computed by hybrid methods and FEM. (Team 3, 50 Hz.)

method	Re(b_{Σ_1})	Im(b_{Σ_1})	Re(b_{Σ_2})	Im(b_{Σ_2})
a-φ	6.92	−2.10	6.93	−2.09
a, v-φ	6.92	−2.10	6.93	−2.09
h-φ	6.91	−2.07	6.92	−2.07
t-φ	6.59	−2.06	6.60	−2.06
2nd ord. FEM	6.59	−2.06	6.60	−2.06

TABLE 6. Magnetic flux (μ T) through cuts Σ_1, Σ_2 in Fig. 3 computed by hybrid methods and FEM. (Team 3, 200 Hz.)

method	Re(b_{Σ_1})	Im(b_{Σ_1})	Re(b_{Σ_2})	Im(b_{Σ_2})
a-φ	3.21	−3.33	3.23	−3.32
a, v-φ	3.21	−3.33	3.23	−3.32
h-φ	3.25	−3.28	3.27	−3.27
t-φ	3.25	−3.28	3.27	−3.27
2nd ord. FEM	2.92	−3.31	2.92	−3.31

TABLE 7. Eddy current (A) through cuts Σ_3, Σ_4 in Fig. 3 computed by hybrid methods and FEM. (Team 3, 50 Hz.)

method	Re(I_{Σ_3})	Im(I_{Σ_3})	Re(I_{Σ_4})	Im(I_{Σ_4})
a-φ	−21.26	−62.27	21.28	62.05
a, v-φ	−21.26	−62.27	21.28	62.05
h-φ	−21.12	−61.46	21.11	61.43
t-φ	−21.12	−61.45	21.11	61.45
2nd ord. FEM	−20.76	−61.80	20.76	61.80

B. TOROIDAL TRANSFORMER

The multigrid-based algorithm is tested on a model with knotted geometry, which cannot be treated efficiently by Gmsh.

TABLE 8. Eddy current (A) through cuts Σ_3, Σ_4 in Fig. 3 computed by hybrid methods and FEM. (Team 3, 200 Hz.)

method	$\mathrm{Re}(I_{\Sigma_3})$	$\mathrm{Im}(I_{\Sigma_3})$	$\mathrm{Re}(I_{\Sigma_4})$	$\mathrm{Im}(I_{\Sigma_4})$
a-φ	−131.38	−98.18	131.35	97.20
a, v-φ	−131.17	−98.06	130.97	96.95
h-φ	−129.82	−95.89	129.75	95.82
t-φ	−129.80	−95.87	129.67	95.77
2nd ord. FEM	−130.70	−98.76	130.70	98.77

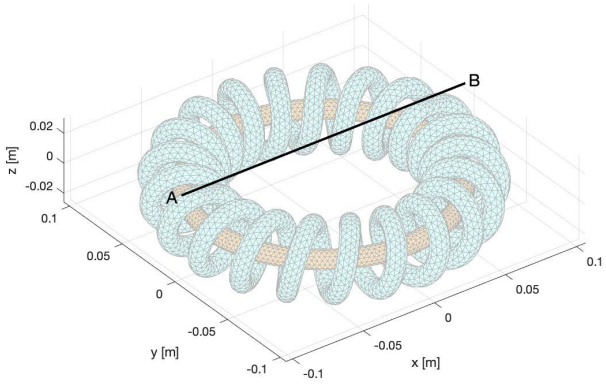

FIGURE 8. Toroidal transformer: a solenoid ($\beta_1 = 1$) is excited by a current loop centered on the same axis. The magnetic flux density is computed along the line AB located above the spiral coil at $z = 30$ mm.

The model shown in Fig. 8 consists of a toroidal conductor with spiral shape (32.78 MS/m conductivity, $\mu_r = 1$ relative permeability, 21 turns), with 20 mm minor radius and 80 mm major radius, which is excited by an AC current-driven loop (1 MA/m^2 current density, 50 Hz frequency, 80 mm radius). Both windings of the toroidal transformer have the same circular cross-section (6 mm radius). The conductive region is multiply connected since it is homeomorphic to a donought, with $\beta_1 = 1$; therefore, Algorithm 1 searches for only one cohomology generator. The whole model is embedded into a cube of 1 m side to exclude boundary effects on the field calculations. The transformer model is fully three-dimensional since the spiral coil does not exhibit any kind of symmetry. The origin of the Cartesian reference frame (x, y, z) is centered on the loop axis; distances are all expressed in millimeters. The magnetic flux density is computed along the horizontal line AB, which goes from point A (−100,0,30) to point B (100,0,30).

Numerical tests similar to the Team 3 problem were carried out to assess the complexity of AGMGcc-based solvers for different mesh refinements. CPU time for computing the source field by solving the curl-curl linear system (30) is considered in Table 9. The number of iterations of AGMGcc

TABLE 9. Computational performance of source field generation for different meshes. (Toroidal transformer.)

# tets	CPU time (s) (solution)	AGMGcc # DOFs	AGMGcc # iterations
634 835	7.03	742 569	20
1 115 336	12.12	1 311 783	20
2 212 157	23.76	2 602 101	20
3 111 747	37.32	3 658 356	24

TABLE 10. Computational performance of multigrid-based algorithm for different meshes. (Toroidal transformer.)

# tets	CPU time (s) (generation)	AGMGcc # DOFs	AGMGcc # iterations
634 835	28.00	683 714	118
1 115 336	52.29	1 252 928	116
2 212 157	105.81	2 543 246	112
3 111 747	155.16	3 599 501	116

solver remains constant up to a few millions DOFs; therefore computational complexity is again optimal. Despite a much more complex model geometry compared to that of Team 3 problem, the computational time is comparable.

Computational performance of multigrid-based algorithm was evaluated for the same mesh refinements. The relative tolerance for AGMGcc and AGMG solvers was fixed to 10^{-10} as in the previous benchmark. Table 10 shows that cohomology is computed by multigrid-based algorithm in a few tens of seconds even for curl-curl linear systems of a few millions elements. This could not be computed by using Gmsh software in a reasonable computing time, being based on large integer matrix computations. Compared to Team 3 problem the number of AGMGcc iterations and CPU time are greater. It is interesting to observe that the computational complexity is again optimal, since the number of AGMGcc iterations remains almost constant when refining the mesh. This behavior is clearly proven by Fig. 9, where dashed line indicates the reference $\mathcal{O}(N)$ complexity. Note that optimal complexity is attained for completely different models, which shows the robustness of the proposed multigrid-based algorithm for computing cohomology generators. As mentioned above, this is achieved in the new version of the algorithm by avoiding the use of Dirichlet BCs.

Numerical tests considered in the following are based on the same discretized model with 634 835 tetrahedrons (59 775 of which are used to mesh the conductive domain in order to capture the skin effect inside the plate at 50 Hz).

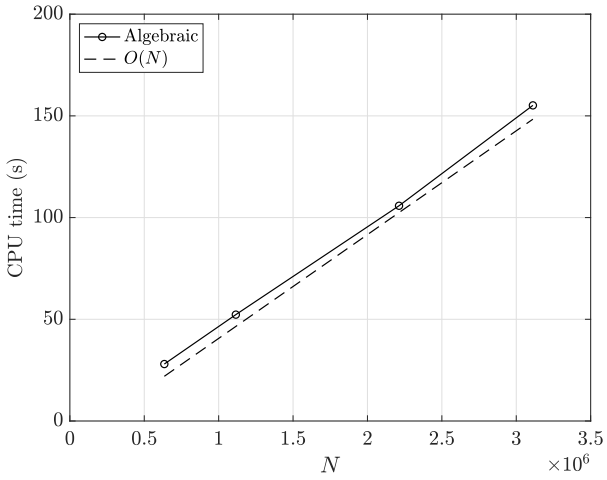

FIGURE 9. Computational time-complexity of multigrid-based algorithm: CPU time (s) vs. number of tetrahedrons N; linear complexity is in dashed line. (Toroidal transformer.)

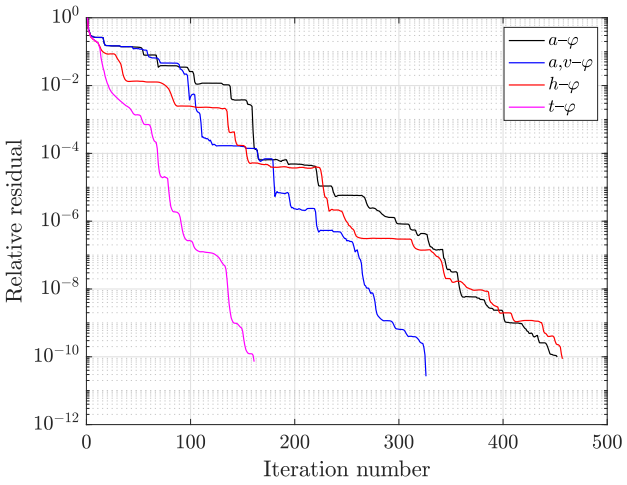

FIGURE 10. Convergence pattern of TFQMR solver for hybrid methods. (Toroidal transformer.)

TABLE 11. Computational performance of hybrid methods for the coarsest mesh in Table 9. (Toroidal transformer.)

method	CPU time (s) (assembly)	CPU time (s) (solution)	TFQMR # DOFs	TFQMR # iterations
a-φ	50.96	19.33	181 753	452
a, v-φ	52.75	19.95	196 280	326
h-φ	54.03	18.38	158 581	457
t-φ	53.06	7.62	165 384	161

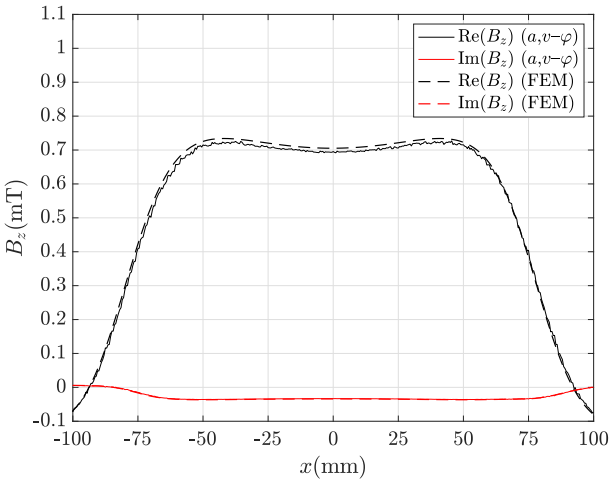

FIGURE 11. Real and imaginary parts of the magnetic flux density (z-axis component) computed along the line AB in Fig. 8 by using the a, v-φ formulation.

Table 11 shows a comparison of the computing performance of different hybrid formulations by considering the CPU time needed for the final linear system assembly and its solution by TFQMR+SSOR iterative solver. It can be observed again that t-φ formulation shows the best performance in terms of CPU time for solution and number of iterations. The final linear system of this formulation was solved in 7.62 s, which is less than a half of the solution time experienced by the other formulations. This value is also comparable to that obtained with the Team 3 model simulations.

Fig. 10 shows that all formulations exhibit a smooth convergence pattern. In particular, the t-φ formulation attains in 161 iterations 10^{-10} relative tolerance, which is a value comparable to that obtained in the Team 3 benchmark.

To verify the accuracy of proposed numerical methods, the z–component of the magnetic flux density (real and imaginary parts) was computed in 401 equally spaced points along the line AB in Fig. 8. The reference solution was obtained by a commercial software implementing the A, V-A formulation with second-order FEM discretization, as in the previous benchmark. The FEM linear system (with 4 026 890 DOFs) was solved by TFQMR with geometric multigrid preconditioner. This solver attained the fixed tolerance of 10^{-10} in 544 s. To stabilize the FEM solver a fake conductance of 1 S/m had to be adopted in the air region, which may slightly affect the solution accuracy. This is not required when using hybrid formulations. Fig. 11 shows that the real and imaginary parts of the magnetic flux density z–component of a, v-φ formulation are in very good agreement with the same profiles obtained by second-order FEM. In this case the maximum discrepancy is 2.84% for the real part and 5.46% for the imaginary part. Comparable levels of accuracy were obtained by considering the other hybrid formulations. It should be noted as in the case of Team 3 benchmark that hybrid formulations provide accurate results with far less DOFs than those of the FEM and also their solution time is negligible compared to that of the FEM.

VI. CONCLUSION

A novel multigrid-based algorithm for finding cohomology in linear-time has been proposed. The procedure is based on

an algebraic multigrid solver for curl-curl field problems. Its main advantage is that costly integer matrix computations and mesh reduction algorithms can be avoided. Numerical experiments further demonstrate a remarkable flexibility of the multigrid-based algorithm, which allows for an easy treatment of models with complex topology. The fast computation of cohomology generators has made it possible to develop efficient hybrid formulations for simulating eddy current problems with multiply connected insulating domains. Novel a, v-φ and t-φ hybrid formulations show much better numerical performance than a-φ and h-φ formulations, while attaining the same level of accuracy. These techniques allow the eddy current model to be represented with a minimum amount of DOFs, with great savings in terms of computational cost compared to classical A, V-A formulation typically implemented in FEM commercial software for EM design. Novel hybrid formulations also overcome typical drawbacks of the T-Ω method when facing multiply connected field problems.

REFERENCES

[1] O. Bíró, "Edge element formulations of eddy current problems," *Comput. Methods Appl. Mech. Eng.*, vol. 169, nos. 3–4, pp. 391–405, 1999.

[2] E. E. Kriezis, T. D. Tsiboukis, S. M. Panas, and J. A. Tegopoulos, "Eddy currents: Theory and applications," *Proc. IEEE*, vol. 80, no. 10, pp. 1559–1589, Oct. 1992.

[3] T. Preston and A. Reece, "Solution of 3-dimensional eddy current problems: The T-Ω method," *IEEE Trans. Magn.*, vol. MAG-18, no. 2, pp. 486–491, Mar. 1982.

[4] P. R. Kotiuga, "On making cuts for magnetic scalar potentials in multiply connected regions," *J. Appl. Phys.*, vol. 61, no. 8, pp. 3916–3918, Apr. 1987.

[5] A. A. Rodríguez, E. Bertolazzi, R. Ghiloni, and A. Valli, "Finite element simulation of eddy current problems using magnetic scalar potentials," *J. Comput. Phys.*, vol. 294, pp. 503–523, Aug. 2015.

[6] J. C. Crager and P. R. Kotiuga, "Cuts for the magnetic scalar potential in knotted geometries and force-free magnetic fields," *IEEE Trans. Magn.*, vol. 38, no. 2, pp. 1309–1312, Mar. 2002.

[7] J. Simkin, S. C. Taylor, and E. X. Xu, "An efficient algorithm for cutting multiply connected regions," *IEEE Trans. Magn.*, vol. 40, no. 2, pp. 707–709, Mar. 2004.

[8] L. Kettunen, K. Forsman, and A. Bossavit, "Formulation of the eddy current problem in multiply connected regions in terms ofh," *Int. J. Numer. Methods Eng.*, vol. 41, no. 5, pp. 935–954, Mar. 1998.

[9] Z. Ren, "T-Ω formulation for eddy-current problems in multiply connected regions," *IEEE Trans. Magn.*, vol. 38, no. 2, pp. 557–560, Mar. 2002.

[10] P. Zhou, Z. Badics, D. Lin, and Z. Cendes, "Nonlinear T-ω formulation including motion for multiply connected 3-D problems," *IEEE Trans. Magn.*, vol. 44, no. 6, pp. 718–721, Jun. 2008.

[11] F. Henrotte and K. Hameyer, "An algorithm to construct the discrete cohomology basis functions required for magnetic scalar potential formulations without cuts," *IEEE Trans. Magn.*, vol. 39, no. 3, pp. 1167–1170, May 2003.

[12] S. Peltier, S. Alayrangues, L. Fuchs, and J.-O. Lachaud, "Computation of homology groups and generators," *Comput. Graph.*, vol. 30, no. 1, pp. 62–69, Feb. 2006.

[13] M. Pellikka, S. Suuriniemi, and L. Kettunen, "Homology in electromagnetic boundary value problems," *Boundary Value Problems*, vol. 2010, no. 1, 2010, Art. no. 381953.

[14] M. Pellikka, S. Suuriniemi, L. Kettunen, and C. Geuzaine, "Homology and cohomology computation in finite element modeling," *SIAM J. Sci. Comput.*, vol. 35, no. 5, pp. B1195–B1214, Jan. 2013.

[15] C. Geuzaine and J.-F. Remacle. *GMSH: A Three-Dimensional Finite Element Mesh Generator With Built-in Pre- and Post-Processing Facilities*. Accessed: Jul. 2, 2022. [Online]. Available: http://gmsh.info/

[16] F. Moro, J. Smajic, and L. Codecasa, "A novel h—φ approach for solving eddy–current problems in multiply connected regions," *IEEE Access*, vol. 8, pp. 170659–170671, 2020.

[17] F. Moro, A. Napov, and L. Codecasa, "A hybrid a–φ cell method for solving eddy-current problems in 3–d multiply–connected domains," *IEEE Access*, vol. 9, pp. 158247–158258, 2021.

[18] A. Napov. *AGMG_CC: AGgregation-Based Algebraic MultiGrid Preconditioners for Curl-Curl Discretization*. Accessed: Aug. 10, 2022. [Online]. Available: http://metronu.ulb.ac.be/AGMG_CC

[19] F. Moro and L. Codecasa, "Coupling the cell method with the boundary element method in static and quasi–static electromagnetic problems," *Mathematics*, vol. 9, no. 12, p. 1426, Jun. 2021.

[20] Z. Ren, C. Li, and A. Razek, "Hybrid FEM-BIM formulation using electric and magnetic variables," *IEEE Trans. Magn.*, vol. 28, no. 2, pp. 1647–1650, Mar. 1992.

[21] A. A. Rodríguez, R. Hiptmair, and A. Valli, "A hybrid formulation of eddy current problems," *Numer. Methods Partial Differ. Equ.*, vol. 21, no. 4, pp. 742–763, 2005.

[22] R. Hiptmair and O. Sterz, "Current and voltage excitations for the eddy current model," *Int. J. Numer. Model.*, vol. 18, pp. 1–21, Jan./Feb. 2005.

[23] A. A. Rodríguez, E. Bertolazzi, R. Ghiloni, and A. Valli, "Construction of a finite element basis of the first de rham cohomology group and numerical solution of 3D magnetostatic problems," *SIAM J. Numer. Anal.*, vol. 51, no. 4, pp. 2380–2402, Jan. 2013.

[24] N. Douglas, *Finite Element Exterior Calculus*. Philadelphia, PA, USA: SIAM, 2018.

[25] Y. Notay, "Flexible conjugate gradients," *SIAM J. Sci. Comput.*, vol. 22, no. 4, pp. 1444–1460, Jan. 2000.

[26] R. Hiptmair and J. Xu, "Auxiliary space preconditioning for edge elements," *IEEE Trans. Magn.*, vol. 44, no. 6, pp. 938–941, Jun. 2008.

[27] T. Kolev and P. Vassilevski, "Some experience with a H^1–based auxiliary space AMG for H(curl) problems," LLNL, Livermore, CA, USA, Tech. Rep. UCRL-TR-221841, 2006.

[28] Y. Notay, "An aggregation-based algebraic multigrid method," *Electron. Trans. Numer. Anal.*, vol. 37, pp. 123–146, Oct. 2010.

[29] L. Codecasa and M. Politi, "Explicit, consistent, and conditionally stable extension of FD-TD to tetrahedral grids by FIT," *IEEE Trans. Magn.*, vol. 44, no. 6, pp. 1258–1261, Jun. 2008.

[30] A. Kameari, "Three dimensional eddy current calculation using edge elements for magnetic vector potential," in *Applied Electromagnetics in Materials*, K. Miya, Ed. New York, NY, USA: Pergamon, 1989, pp. 225–236.

[31] International Compumag Society. *Problem 3: Bath Plate With Two Holes*. Accessed: Sep. 4, 2022. [Online]. Available: https://www.compumag.org/jsite/images/stories/TEAM/problem3.pdf

[32] D. Rodger, "BENCHMARK PROBLEM 3 (THE BATH PLATE)," *COMPEL-Int. J. Comput. Math. Electr. Electron. Eng.*, vol. 7, nos. 1–2, pp. 47–63, Jan. 1988.

FEDERICO MORO (Senior Member, IEEE) received the Laurea degree in electrical engineering, the Ph.D. degree in bioelectromagnetic and electromagnetic compatibility, and the B.S. degree in mathematics from the University of Padova, Italy, in 2003, 2007, and 2012. He was a Visiting Scholar at the Department of Physics, Swansea University, Wales, U.K., in 2005 and a Visiting Professor at the G2ELab, Grenoble, France, in 2020. From 2007 to 2010, he was a Research Associate at the Department of Electrical Engineering, University of Padova. From 2010 to 2020, he was an Assistant Professor of electrical engineering at the Department of Industrial Engineering, University of Padova. Since 2020, he has been working as an Associate Professor of electrical engineering with the Department of Industrial Engineering. He is the author of more than 100 articles in peer-reviewed international journals and conference proceedings. His research interests include numerical methods for computing electromagnetic problems and the numerical modeling of multiphysics and multiscale problems. He was awarded the Best Oral Presentation at UPEC, 2006, and the Best Paper at ASME IDETC/CIE 2017 and 2022, and Electrimacs 2019 conferences. He obtained the National Scientific Qualification as a Full Professor (09/E1-Elettrotecnica) in 2021.

ARTEM NAPOV received the Ph.D. degree in engineering from the Université libre de Bruxelles (ULB), in 2010. From 2010 to 2012, he was a Postdoctoral Fellow at the Computational Science Division of Lawrence Berkeley National Laboratory. Since 2012, he has been working with the École poytechnique de Bruxelles (ULB), first as an Assistant Professor, where he is an Associate Professor, since 2017. His research interest includes numerical methods for the solution of large sparse linear systems of equations arising from PDE discretizations.

MATTI PELLIKKA was born in 1984. He received the Ph.D. degree from the Tampere University of Technology, in 2014. Since then, he has been working as an Algorithm Engineer with Nokia, Microsoft, and Grundium. His research interests include applied mathematics, multiphysics modeling, and image processing.

JASMIN SMAJIC (Senior Member, IEEE) received the B.Sc. degree from the Faculty of Electrical Engineering, Tuzla, Bosnia and Herzegovina, in 1996, the M.Sc. and the Ph.D. degrees from the Faculty of Electrical Engineering and Computing, Zagreb, Croatia, in 1998 and 2001, respectively. The main topic of the M.Sc. and Ph.D. degrees was numerical computing of static and time-varying electromagnetic fields in power transformers and electrical machines, as well as their design optimization. The main topics of the Ph.D. degree were full-Maxwell electromagnetic simulations of photonic crystals and similar electromagnetic meta-materials. From 2002 to 2004, he was a Postdoctoral Research Fellow at the Computational Optics Group of the Laboratory for Electromagnetic Fields and Microwave Electronics, ETH Zurich (Switzerland). In 2004, he took a position of scientist at the ABB Corporate Research Centre, Baden-Dättwil (Switzerland), where he stayed until 2011. His work in ABB covered a wide range of projects in the field of computational and applied electromagnetics such as LI-modeling and simulation of transformer windings, fast electromagnetic transients in power and distribution transformers, coupled electromagnetic-mechanical and electromagnetic-thermal analysis of transformers and circuit breakers, and very fast electromagnetic transients in gas insulated switchgears. From 2007 to 2020, he was an External Lecturer at the Swiss Federal Institute of Technology (ETH) Teaching at the master's and Ph.D. level several courses on computational electromagnetics and physical modeling. From 2011 to 2020, he was a Professor of electrical engineering at the University of Applied Sciences, Rapperswil (Switzerland), where he was leading the Computational and Applied Electromagnetics Group (CAEM). Since 2020, he has been a Lecturer and a Senior Scientist with the Swiss Federal Institute of Technology (ETH), Zurich. At Institute of Electromagnetic Fields (IEF) he is currently leading theoretical and simulation related research activities. He has authored more than 100 articles and dozens of patents. He is a member of CIGRE.

LORENZO CODECASA (Member, IEEE) received the Ph.D. degree in electronic engineering from the Politecnico di Milano, in 2001. From 2002 to 2010, he worked as an Assistant Professor of electrical engineering at the Department of Electronics, Information, and Bioengineering, Politecnico di Milano, where he has been working as an Associate Professor of electrical engineering, since 2010. His main research contributions are in the theoretical analysis and in the computational investigation of electric circuits and electromagnetic fields. In his research on heat transfer and thermal management of electronic components, he has introduced original industrial-strength approaches to the extraction of compact thermal models, currently available in market leading commercial software. For these activities, he received the Harvey Rosten Award for Excellence, in 2016. He has been serving as an Associate Editor for the IEEE TRANSACTIONS OF COMPONENTS, PACKAGING, AND MANUFACTURING TECHNOLOGY. He has also been serving as the Chair of the conference Thermal Investigations of Integrated Circuits (THERMINIC). He has authored or coauthored over 200 papers in refereed international journals and conference proceedings in his research areas.

Open Access funding provided by 'Università del Salento' within the CRUI CARE Agreement